Supplemental Material for "Magnon-Skyrmion Hybrid Quantum Systems: Tailoring Interactions via Magnons"

Xue-Feng Pan,[1] Peng-Bo Li,[1,*] Xin-Lei Hei,[1] Xichao Zhang,[2] Masahito Mochizuki,[2] Fu-Li Li,[1] and Franco Nori[3,4,5]

[1] *Ministry of Education Key Laboratory for Nonequilibrium Synthesis and Modulation of Condensed Matter, Shaanxi Province Key Laboratory of Quantum Information and Quantum Optoelectronic Devices, School of Physics, Xi'an Jiaotong University, Xi'an 710049, China*

[2] *Department of Applied Physics, Waseda University, Okubo, Shinjuku-ku, Tokyo 169-8555, Japan*

[3] *Theoretical Quantum Physics Laboratory, Cluster for Pioneering Research, RIKEN, Wakoshi, Saitama 351-0198, Japan*

[4] *Center for Quantum Computing, RIKEN, Wakoshi, Saitama 351-0198, Japan*

[5] *Physics Department, The University of Michigan, Ann Arbor, Michigan 48109-1040, USA*

(Dated: April 10, 2024)

In this supplemental material, we first present some details about spin-wave quantization and skyrmion quantization in Sec. I and Sec. II, respectively. Sec. III offers a detailed derivation of the coupling strength of the magnon and the magnetic skyrmion qubit. In Sec. IV, the coupling between skyrmion qubits is evaluated. In addition, we extend the derivation of the magnon Kerr effect and introduce a two-magnon drive. Section V calculates the magnon-mediated non-reciprocal dissipative coupling between skyrmion qubits. In Sec. VI and Sec. VII, a detailed analysis of the skyrmion-magnon-NV and skyrmion-magnon-SQ hybrid quantum systems is presented. The micromagnetic simulation of the hybrid system proposed here is elaborated in Sec. VIII. In Sec. IX, the coupling model based on magnetic multilayer structures is discussed in detail.

CONTENTS

* lipengbo@mail.xjtu.edu.cn

I. THE SPIN WAVE

In this section, we solve for the spin waves in spherical magnets and the quantization of the magnon. First, we start from the nonlinear Landau-Lifschitz (LL) equation and obtain the linear LL magnetostatic dipolar spin wave equations by some reasonable physical approximations. Then we calculate the eigenmode of the spin-wave equation. Finally, we quantize the spin wave and evaluate the relevant parameters for the Kittel mode. In the subsequent calculation, we establish the local coordinate xyz with the YIG spherical center as the coordinate origin.

A. The spin-wave equation

Here we focus on the spin waves supported by a micromagnetic sphere. They can be described by the continuous magnetization field $\boldsymbol{M}(\boldsymbol{r},t)$ with related electromagnetic fields $\boldsymbol{E}(\boldsymbol{r},t)$ and $\boldsymbol{H}(\boldsymbol{r},t)$, which follow the Maxwell equations and the phenomenological nonlinear LL equation [1, 2]

$$\partial_t \boldsymbol{M}(\boldsymbol{r},t) = -|\gamma_e|\mu_0 \boldsymbol{M}(\boldsymbol{r},t) \times \boldsymbol{H}_{\text{eff}}(\boldsymbol{M},\boldsymbol{r},t), \tag{1}$$

where $\boldsymbol{H}_{\text{eff}} = \boldsymbol{H}(\boldsymbol{r},t) + \Delta\boldsymbol{H}(\boldsymbol{M},\boldsymbol{r},t)$ is the effective field. The external field $\Delta\boldsymbol{H}$ includes the exchange field, the magnetocrystalline anisotropy field, and the demagnetizing field due to the dipole-dipole interaction, which can be written as [2]

$$\Delta\boldsymbol{H}(\boldsymbol{M},\boldsymbol{r},t) = \boldsymbol{H}_{\text{ex}}(\boldsymbol{M},\boldsymbol{r},t) + \boldsymbol{H}_{\text{an}}(\boldsymbol{M},\boldsymbol{r},t) + \boldsymbol{H}_{\text{dm}}(\boldsymbol{M},\boldsymbol{r},t). \tag{2}$$

In general, the contribution of the external field $\Delta\boldsymbol{H}$ is related to the magnetization $\boldsymbol{M}$, which leads to the nonlinearity of the LL equation and makes the quantization of spin waves very difficult. In the following, we use three approximations to linearize the nonlinear LL equation to obtain the spin-wave equation. (i) Spin-wave approximation. Applying a sufficiently large magnetic field B_K in the z direction to the magnetic sphere, which ensures saturation magnetization of the magnetic sphere, we can then write the physical field as the saturation term plus its corresponding fluctuation

$$\begin{aligned} \boldsymbol{H}(\boldsymbol{r},t) &= H_0\boldsymbol{e}_z + \boldsymbol{h}(\boldsymbol{r},t), \\ \boldsymbol{M}(\boldsymbol{r},t) &= M_s\boldsymbol{e}_z + \boldsymbol{m}(\boldsymbol{r},t), \end{aligned} \tag{3}$$

where the fluctuation terms satisfy $\boldsymbol{h} \ll H_0$ and $\boldsymbol{m} \ll M_s$. Then the LL equation (1) can be reduced to

$$\frac{1}{|\gamma_e|\mu_0 M_s H_0}\partial_t \boldsymbol{m}(\boldsymbol{r},t) - \boldsymbol{e}_z \times \left[\frac{\boldsymbol{m}(\boldsymbol{r},t)}{M_s} - \frac{\boldsymbol{h}(\boldsymbol{r},t)}{H_0}\right] + \left[\boldsymbol{e}_z + \frac{\boldsymbol{m}(\boldsymbol{r},t)}{M_s}\right] \times \frac{\Delta\boldsymbol{H}(\boldsymbol{M},\boldsymbol{r},t)}{H_0} = \frac{\boldsymbol{m}(\boldsymbol{r},t)}{M_s} \times \frac{\boldsymbol{h}(\boldsymbol{r},t)}{H_0}. \tag{4}$$

Retaining only the first order terms of the small quantities $\boldsymbol{m}(\boldsymbol{r},t)/M_s$ and $\boldsymbol{h}(\boldsymbol{r},t)/H_0$, the LL equation can be written as

$$\frac{1}{|\gamma_e|\mu_0 M_s H_0}\partial_t \boldsymbol{m}(\boldsymbol{r},t) - \boldsymbol{e}_z \times \left[\frac{\boldsymbol{m}(\boldsymbol{r},t)}{M_s} - \frac{\boldsymbol{h}(\boldsymbol{r},t)}{H_0}\right] + \left[\frac{\boldsymbol{m}(\boldsymbol{r},t)}{M_s}\right] \times \frac{\Delta\boldsymbol{H}(\boldsymbol{M},\boldsymbol{r},t)}{H_0} = 0. \tag{5}$$

It is worth noting that for the first-order term $\boldsymbol{m}(\boldsymbol{r},t)/M_s$, we can obtain $\boldsymbol{m}(\boldsymbol{r},t)\cdot\boldsymbol{e}_z = 0$. (ii) External field $\Delta\boldsymbol{H}(\boldsymbol{M},\boldsymbol{r},t)$. When the size of the magnetic sphere is much larger than the length of the domain wall, the spin wave is dominated by the dipole-dipole interaction, at which case the exchange interaction can be neglected, i.e., $\boldsymbol{H}_{\text{ex}} \approx 0$ [1, 2]. For cubic materials, the magnetocrystalline anisotropy is given by $\boldsymbol{H}_{\text{an}} = -(2K_{\text{an}}/M_s^2)M_z\boldsymbol{e}_z$, i.e., the contribution of $\boldsymbol{H}_{\text{an}}$ to the LL equation is a second-order small quantity $(\boldsymbol{m}/M_s)^2$ [1, 2], indicating that the effect of magnetocrystalline anisotropy can be neglected. The demagnetizing field of a uniformly magnetized ellipsoid can be written as $\boldsymbol{H}_{\text{dm}} = -(N_x M_s^x, N_y M_s^y, N_z M_s^z)$ where $N_{x,y,z}$ represents the static magnetic factor and it satisfies $N_x + N_y + N_z = 1$. For different geometries, the static magnetic factor takes different values: for a thin film in the xz plane, $N_x = N_z = 0, N_y = 1$, for a cylindrical line along the z direction, $N_x = N_y = 1/2, N_z = 0$, and for a spherical magnet, $N_x = N_y = N_z = 1/3$. Here we can write the demagnetizing field as a simple form $\boldsymbol{H}_{\text{dm}} = -M_s\boldsymbol{e}_z/3$ [1, 3]. With these external field approximations, the LL equations (5) for the different components are expressed as [2]

$$\begin{aligned} \partial_t m_x(\boldsymbol{r},t) &= -\omega_0 m_y(\boldsymbol{r},t) + \omega_M h_y(\boldsymbol{r},t), \\ \partial_t m_y(\boldsymbol{r},t) &= \omega_0 m_x(\boldsymbol{r},t) - \omega_M h_x(\boldsymbol{r},t), \end{aligned} \tag{6}$$

where two relevant system frequencies and the internal field are defined as $\omega_0 \equiv |\gamma_e|\mu_0 H_I$, $\omega_M \equiv |\gamma_e|\mu_0 M_s$, and $H_I \equiv H_0 - 1/3M_s$, respectively. (iii) Magnetostatic approximation $\nabla \times \boldsymbol{h}(\boldsymbol{r},t) = 0$. With this approximation, the

electric field component and the magnetic field component $\boldsymbol{h}$ of the spin wave are decoupled, which results in the electric field component being negligible. In addition, we can also introduce a static magnetic potential $\psi(\boldsymbol{r},t)$, defined as $\boldsymbol{h}(\boldsymbol{r},t)=-\nabla\psi(\boldsymbol{r},t)$. According to the zero-divergence condition $\nabla\cdot\boldsymbol{b}(\boldsymbol{r},t)=0$ and $\boldsymbol{b}(\boldsymbol{r},t)=\mu_0[\boldsymbol{h}(\boldsymbol{r},t)+\boldsymbol{m}(\boldsymbol{r},t)]$, we can obtain the equation of the static magnetic potential

$$\nabla^2\psi(\boldsymbol{r},t)=\partial_x m_x(\boldsymbol{r},t)+\partial_y m_y(\boldsymbol{r},t). \tag{7}$$

The equations (6) and (7) allow for the analysis of the interior of the magnetic sphere. For the exterior of the magnetic sphere, the scalar field $\psi(\boldsymbol{r},t)$ satisfies

$$\nabla^2\psi(\boldsymbol{r},t)=0. \tag{8}$$

B. Solving the spin-wave equation: Walker modes

The Walker modes of the micromagnetic sphere will be calculated hereafter. The eigenmodes of the magnetization intensity and magnetic field are $\boldsymbol{m}_\beta(\boldsymbol{r})$ and $\boldsymbol{h}_\beta(\boldsymbol{r})=-\nabla\psi_\beta(\boldsymbol{r})$. Then, similar to the electromagnetic field quantization, the corresponding field can be expressed as [4, 5]

$$\begin{aligned}\boldsymbol{m}(\boldsymbol{r},t)&=\sum_\beta\left[s_\beta\boldsymbol{m}_\beta(\boldsymbol{r})\,e^{-i\omega_\beta t}+c.c\right],\\ \boldsymbol{h}(\boldsymbol{r},t)&=\sum_\beta\left[s_\beta\boldsymbol{h}_\beta(\boldsymbol{r})\,e^{-i\omega_\beta t}+c.c\right],\end{aligned} \tag{9}$$

where s_β is the complex amplitude, the mode index is β, and the eigenfrequency is ω_β. Substituting Eq. (9) into LL equation (6) results in

$$\begin{aligned}i\omega m_x(\boldsymbol{r})&=\omega_M\partial_y\psi(\boldsymbol{r})+\omega_0 m_y(\boldsymbol{r}),\\ i\omega m_y(\boldsymbol{r})&=-\omega_M\partial_x\psi(\boldsymbol{r})-\omega_0 m_x(\boldsymbol{r}).\end{aligned} \tag{10}$$

Replacing the linear LL equation (10) into the scalar field equation (7) we can obtain the equation that contains only the static magnetic potential. In summary, we can obtain the equations for the scalar field inside and outside the magnetic sphere, given by

$$(1+\chi_p)\left(\partial_x^2+\partial_y^2\right)\psi_{\rm in}(\boldsymbol{r})+\partial_z^2\psi_{\rm in}(\boldsymbol{r})=0, \tag{11a}$$

$$\nabla^2\psi_{\rm out}(\boldsymbol{r})=0. \tag{11b}$$

$\psi_{\rm in}$ and $\psi_{\rm out}$ are the static magnetic potential inside and outside the magnetic sphere, respectively. The diagonal element of the Polder susceptibility tensor is defined as $\chi_p(\omega)=\omega_M\omega_0/(\omega_0^2-\omega^2)$ [2]. Hereafter we solve the equations of static magnetic potential $\psi(\boldsymbol{r})$ outside and inside the magnetic sphere. Outside the magnetic sphere, the static magnetic potential follows Eq. (11b), using the spherical harmonic functions $Y_l^m(\theta,\phi)$ in spherical coordinates $\boldsymbol{r}=(r,\theta,\phi)$, whose general solution can be written as

$$\psi_{\rm out}(\boldsymbol{r})=\sum_{l,m}\left[\frac{A_{l,m}}{r^{l+1}}+B_{l,m}r^l\right]Y_l^m(\theta,\phi). \tag{12}$$

The expansion coefficients $A_{l,m}$ and $B_{l,m}$ can be determined by boundary conditions. According to the boundary condition: the static magnetic potential is regular, i.e., it is convergent at infinity [$\psi_{\rm out}(r\to\infty)\to 0$], then the coefficient $B_{l,m}=0$ can be obtained. Inside the magnetic sphere, the static magnetic potential satisfies Eq. (11a). For convenience, a set of orthogonal coordinates $\{\xi,\eta,\phi\}$ is introduced, defined as $x=\sqrt{\chi_p}R\sqrt{\xi^2-1}\sin\eta\cos\phi$, $y=\sqrt{\chi_p}R\sqrt{\xi^2-1}\sin\eta\sin\phi$, and $z=\sqrt{\chi_p/(1+\chi_p)}R\xi\cos\eta$. It is worth noting that the orthogonal coordinates $\{\xi,\eta,\phi\}$ on the surface of the sphere can be simplified to $\xi\to\xi_0=\sqrt{(1+\chi_p)/\chi_p}$, $\eta\to\theta$, and $\phi\to\phi$. In orthogonal coordinates $\{\xi,\eta,\phi\}$, the general solution of the static magnetic potential inside the sphere can be expressed by associated Legendre polynomials and spherical harmonic functions [4, 5]

$$\psi_{\rm in}(\boldsymbol{r})=\sum_{l,m}C_{l,m}P_l^m(\xi)Y_l^m(\eta,\phi) \tag{13}$$

with expansion coefficient $C_{l,m}$. We subsequently use the continuity condition at the surface of the sphere to determine the coefficients. (i) The continuity condition for the tangential component of $\boldsymbol{h}$, i.e., the potential crosses the surface continuously $\psi_{\rm out}|_{r=R} = \psi_{\rm in}|_{\xi=\xi_0}$. Then we can get $A_{l,m} = C_{l,m}P_l^m(\xi_0)R^{l+1}$. (ii) The continuity condition for the normal component of the $\boldsymbol{b}$ field [4]

$$\partial_r\psi_{\rm out}|_{r=R} = \frac{\xi_0}{R}\partial_\xi\psi_{\rm in}|_{r=R} - i\frac{\kappa_p}{R}\partial_\phi\psi_{\rm in}|_{r=R} \tag{14}$$

with non-diagonal elements of Polder susceptibility tensor $\kappa_p(\omega) = \omega_M\omega/(\omega_0^2 - \omega^2)$ [2]. Then we can obtain the eigenfrequency equation of Walker modes [4, 5]

$$\xi_0(\omega)\frac{P_l'^m\left[\xi_0(\omega)\right]}{P_l^m\left[\xi_0(\omega)\right]} + m\kappa_p(\omega) + l + 1 = 0. \tag{15}$$

It is of interest that the equation does not depend on the radius R_K of the micromagnetic sphere, i.e., the eigenfrequency is not associated with the radius of the magnetic sphere. Besides, there exist non-physical solutions of this equation, e.g. $l = 0$. Given $\{l, m\}$, the eigenfrequency equation has a set of discrete solutions. And then we use n to denote the nth mode, and $n = 0$ to denote the fundamental mode. Here we focus on the Kittel mode, which corresponds to a mode index $\{110\}$.

C. Quantization of the spin-wave modes

Here we discuss the quantization of the spin-wave mode. The micromagnetic energy functional of the Walker modes can be written phenomenologically as

$$E_m\left(\{\boldsymbol{m}\},\{\boldsymbol{h}\}\right) = \frac{\mu_0}{2}\int dV\boldsymbol{m}(\boldsymbol{r},t)\cdot\left[\frac{H_I}{M_s}\boldsymbol{m}(\boldsymbol{r},t) - \boldsymbol{h}(\boldsymbol{r},t)\right]. \tag{16}$$

And it can be demonstrated that by this energy functional, the LL equation can be reproduced. According to Eq. (6), we can obtain

$$h_x(\boldsymbol{r},t) = -\frac{1}{\omega_M}\partial_t m_y(\boldsymbol{r},t) + \frac{\omega_0}{\omega_M}m_x(\boldsymbol{r},t). \tag{17a}$$

$$h_y(\boldsymbol{r},t) = \frac{1}{\omega_M}\partial_t m_x(\boldsymbol{r},t) + \frac{\omega_0}{\omega_M}m_y(\boldsymbol{r},t), \tag{17b}$$

Substituting equations (17a) and (17b) into the energy functional (16) yields

$$E_m\left(\{\boldsymbol{m}\}\right) = \frac{1}{2|\gamma_e|M_s}\int dV\{m_x(\boldsymbol{r},t)\partial_t m_y(\boldsymbol{r},t) - m_y(\boldsymbol{r},t)\partial_t m_x(\boldsymbol{r},t)\}. \tag{18}$$

Employing the eigenmode $\boldsymbol{m}_\beta$ of the magnetization intensity, we can derive

$$m_x(\boldsymbol{r},t) = \sum_\beta\left[s_\beta m_{\beta,x}(\boldsymbol{r})e^{-i\omega_\beta t} + c.c.\right], \tag{19a}$$

$$m_y(\boldsymbol{r},t) = \sum_\beta\left[s_\beta m_{\beta,y}(\boldsymbol{r})e^{-i\omega_\beta t} + c.c.\right], \tag{19b}$$

$$\partial_t m_x(\boldsymbol{r},t) = \sum_\beta\left[-i\omega_\beta s_\beta m_{\beta,x}(\boldsymbol{r})e^{-i\omega_\beta t} + c.c.\right], \tag{19c}$$

$$\partial_t m_y(\boldsymbol{r},t) = \sum_\beta\left[-i\omega_\beta s_\beta m_{\beta,y}(\boldsymbol{r})e^{-i\omega_\beta t} + c.c.\right]. \tag{19d}$$

Then equation (18) can be simplified as

$$E_m\left(\{\boldsymbol{m}\}\right)=\frac{\Lambda_\beta}{2|\gamma_e|\hbar M_s}\sum_\beta \hbar\omega_\beta\left(s_\beta s_\beta^*+c.c.\right), \tag{20}$$

where $\Lambda_\beta=\int dV 2\mathrm{Im}[m_{\beta,y}(\boldsymbol{r})m^*_{\beta,x}(\boldsymbol{r})]$ [6, 7]. As a result, a spin wave mode is formally identical to a one-dimensional harmonic oscillator, so it is possible to quantize the spin wave mode following the quantization method of the one-dimensional harmonic oscillator. First we quantize the amplitude as a magnon operator: $s_\beta\to\hat{s}_\beta$ and $s^*_\beta\to\hat{s}^\dagger_\beta$. Then we choose the appropriate eigenfunction

$$\begin{bmatrix}\boldsymbol{m}_\beta(\boldsymbol{r})\\ \boldsymbol{h}_\beta(\boldsymbol{r})\end{bmatrix}\to M_{\mathrm{zpf}}\begin{bmatrix}\widetilde{\boldsymbol{m}}_\beta(\boldsymbol{r})\\ \widetilde{\boldsymbol{h}}_\beta(\boldsymbol{r})\end{bmatrix} \tag{21}$$

to eliminate the constant factor, where the zero-point magnetization $M_{\mathrm{zpf}}=\sqrt{|\gamma_e|\hbar M_s/\Lambda_\beta}$. Finally, using the commutation relations of bose operators $[\hat{s}_\beta,\hat{s}^\dagger_\beta]=1$, we can obtain the field operators and Hamiltonian after quantization

$$\hat{\boldsymbol{m}}(\boldsymbol{r})=\sum_\beta M_{\mathrm{zpf}}\left(\widetilde{\boldsymbol{m}}_\beta(\boldsymbol{r})\hat{s}_\beta+c.c.\right), \tag{22a}$$

$$\hat{\boldsymbol{h}}(\boldsymbol{r})=\sum_\beta M_{\mathrm{zpf}}\left(\widetilde{\boldsymbol{h}}_\beta(\boldsymbol{r})\hat{s}_\beta+c.c.\right), \tag{22b}$$

$$\hat{H}=\sum_\beta \hbar\omega_\beta\left(\hat{s}^\dagger_\beta\hat{s}_\beta+\frac{1}{2}\right). \tag{22c}$$

D. The Kittel mode

For the Kittel mode, the mode function is

$$\widetilde{\boldsymbol{m}}_K=\boldsymbol{e}_x+i\boldsymbol{e}_y \tag{23}$$

at which case the constant factor and the zero-point magnetization are given by $\Lambda_\beta=2V$ and $M_{\mathrm{zpf}}=\sqrt{\gamma_e\hbar M_s/(2V)}$, respectively. M_s indicates saturation magnetization. The free Hamiltonian of the Kittel mode is

$$\hat{H}_K=\omega_K\hat{s}^\dagger_K\hat{s}_K \tag{24}$$

with $\omega_K=\gamma_e B_K$. B_K is the bias magnetic field.

II. THE SKYRMION

A. The classical skyrmion

Skyrmions are a non-collinear spin texture with a centrosymmetric spiral structure, as shown in FIG. S1(a). The in-plane component s_x (s_y) and the out-of-plane s_z are shown in FIGs. S1(a)[(b)] and (c), respectively. In contrast to skyrmions in chiral materials, the skyrmion in inversion-symmetric (frustrated) magnets has a collective coordinate helicity φ_0 that can be quantized as qubits to implement quantum calculations. According to Ginzburg-Landau theory, its Hamiltonian can be expressed as

$$\mathcal{H}=\int d\widetilde{\boldsymbol{r}}\left[-\frac{\mathcal{J}_1}{2}(\nabla_{\widetilde{\boldsymbol{r}}}\boldsymbol{s})^2+\frac{\mathcal{J}_2a^2}{2}(\nabla^2_{\widetilde{\boldsymbol{r}}}\boldsymbol{s})^2-\frac{H}{a^2}s_z+\frac{K}{a^2}s_z^2\right], \tag{25}$$

where $\widetilde{\boldsymbol{r}}=(\widetilde{\rho},\phi)$ stands for the position vector, a denotes lattice spacing, and $\mathcal{J}_{1/2}$ is the strength of the competing interactions. H and K represent the z-direction magnetic field and easy-axis anisotropy, respectively. For

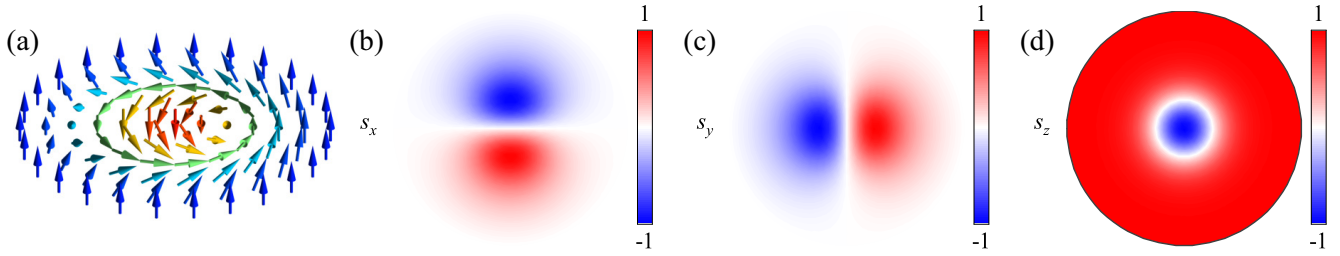

FIG. S1. (a) 3D structure of a skyrmion. (b, c) The in-plane component s_x and s_y of $\boldsymbol{s}$. (d) The out-of-plane component s_z of $\boldsymbol{s}$.

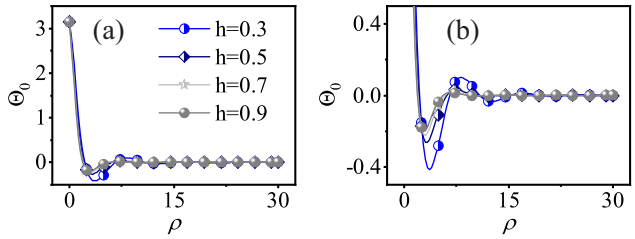

FIG. S2. Approximated solution of the skyrmion.

a classical skyrmion, $\boldsymbol{s} = [\sin\Theta(\widetilde{\rho})\cos\Phi, \sin\Theta(\widetilde{\rho})\sin\Phi, \cos\Theta(\widetilde{\rho})]$, with $\Phi = \phi + \varphi_0$. The stationary skyrmion solution, denoted as Θ_0 and Φ_0, is obtained by minimizing the energy Eq. (25). The radius of the skyrmion is given by $\mathcal{R} = 1/\mathrm{Re}(\mathcal{Y})$ with $\mathcal{Y} = \sqrt{-1+\widetilde{\mathcal{Y}}}/\sqrt{2}$, $\widetilde{\mathcal{Y}} = \sqrt{1-4(h+\kappa_z)}$, $h = H/\mathcal{J}_1$, and $\kappa_z = K/\mathcal{J}_1$. Here, $\Theta_0(\rho) = \pi/\sqrt{\rho^2+1}\exp(-\mathcal{Y}_{\mathrm{Re}}\rho)\cos(\mathcal{Y}_{\mathrm{Im}}\rho)$ with $\mathcal{Y}_{\mathrm{Re}} = \mathrm{Re}(\mathcal{Y})/2$ and $\mathcal{Y}_{\mathrm{Im}} = \mathrm{Im}(\mathcal{Y})/2$ is assumed to be the approximate solution of skyrmions. The approximate solution $\Theta_0(\rho)$ is plotted as a function of ρ for $K = 0$, as depicted in FIG. S2.

B. The skyrmion qubit

1. $\mathfrak{S}_z$ *qubit*

The collective coordinate quantization (in the next section it is shown in detail) is used to derive the Hamiltonian of $\mathfrak{S}_z$ qubits. The real-time action of the skyrmion can be expressed as [8]

$$\mathcal{S} = \frac{\bar{S}}{a^2}\int d\widetilde{t}d\widetilde{\boldsymbol{r}}\dot{\Phi}\left(1-\Pi\right) - \int d\widetilde{t}\mathcal{H}_{\mathfrak{S}_z}, \tag{26}$$

where $\dot{\Phi}$ denotes the first-order derivative with regard to time and $\Pi = \cos\Theta$. The Hamiltonian is

$$\mathcal{H}_{\mathfrak{S}_z} = \bar{S}\int d\widetilde{\boldsymbol{r}}\left[-\frac{H}{a^2}s_z + \frac{K}{a^2}s_z^2 - EP_E a\hat{\boldsymbol{e}}_z\cdot\boldsymbol{P}\right]. \tag{27}$$

Here, we introduce an external electric field that is applied in the z-direction in order to modulate the skyrmion. The electric polarization is represented by $\boldsymbol{P} = \hat{\boldsymbol{e}}_x\times(\boldsymbol{s}\times\partial_{\widetilde{x}}\boldsymbol{s}) + \hat{\boldsymbol{e}}_y\times(\boldsymbol{s}\times\partial_{\widetilde{y}}\boldsymbol{s})$, and P_E is assumed to be 0.2 C/m^2. E is the electric field gradient. With the dimensionless parameters $\mathcal{J}_\Lambda = \mathcal{J}_1$, $\ell = \sqrt{\mathcal{J}_2/\mathcal{J}_1}$, $\widetilde{\boldsymbol{r}} = \boldsymbol{r}\ell a$, and $\widetilde{t} = t/\mathcal{J}_\Lambda$, the action Eq. (26) can be represented as

$$\mathcal{S} = \bar{S}\int dtd\boldsymbol{r}\dot{\Phi}\left(1-\Pi\right) - \int dt\mathcal{H}_{\mathfrak{S}_z}, \tag{28}$$

where

$$\mathcal{H}_{\mathfrak{S}_z} = \int d\boldsymbol{r}\left(-\bar{h}_z s_z + \bar{\kappa}_z s_z^2 - \bar{\varepsilon}_z\hat{\boldsymbol{e}}_z\cdot\bar{\boldsymbol{P}}\right) \tag{29}$$

with $\bar{h}_z = H\bar{S}/\mathcal{J}_\Lambda$, $\bar{\kappa}_z = K\bar{S}/\mathcal{J}_\Lambda$, $\bar{\varepsilon}_z = a^3 E P_E \bar{S}/\mathcal{J}_\Lambda$, and $\bar{\boldsymbol{P}} = \hat{\boldsymbol{e}}_x \times (\boldsymbol{s} \times \partial_x \boldsymbol{s}) + \hat{\boldsymbol{e}}_y \times (\boldsymbol{s} \times \partial_y \boldsymbol{s})$. Utilizing the collective coordinate quantization method presented, we can obtain

$$\begin{aligned} \widetilde{\Pi}(\boldsymbol{r},t) &= \frac{\mathfrak{S}_z - \int d\boldsymbol{r}\eta(\boldsymbol{r},\boldsymbol{t})\partial_\phi \Phi(\boldsymbol{r},t)}{\Lambda}\widetilde{\Pi}_0(\boldsymbol{r},t) + \eta(\boldsymbol{r},t), \\ \Phi(\boldsymbol{r},t) &= \Phi_0\left[\boldsymbol{r},\varphi_0(t)\right] + \xi(\boldsymbol{r},t), \end{aligned} \tag{30}$$

where $\widetilde{\Pi} = 1 - \Pi$ and $\Lambda = \int d\boldsymbol{r}(1 - \cos\Theta_0)$. η and ξ represent the quantum fluctuations of the skyrmion's classical solution. The Hamiltonian of the skyrmion qubit can be expressed in terms of the collective coordinate φ_0 and its conjugate momentum $\mathfrak{S}_z$

$$\mathcal{H}_{\mathfrak{S}_z} = \bar{\bar{\kappa}}_z \mathfrak{S}_z^2 - \bar{\bar{h}}_z \mathfrak{S}_z - \bar{\bar{\varepsilon}}_z \cos\varphi_0. \tag{31}$$

The coefficients in Eq. (31) are defined as

$$\begin{aligned} \bar{\bar{\kappa}}_z &= \bar{\kappa}_z \int d\boldsymbol{r} \frac{(1-\cos\Theta_0)^2}{\int d\boldsymbol{r}\,(1-\cos\Theta_0)^2}, \\ \bar{\bar{h}}_z &= \bar{h}_z, \\ \bar{\bar{\varepsilon}}_z &= \bar{\varepsilon}_z \int d\boldsymbol{r}\left[\partial_\rho \Theta_0 + \frac{\sin(2\Theta_0)}{2\rho}\right]. \end{aligned} \tag{32}$$

Introducing the collective coordinate operator $\hat{\varphi}_0$ and its conjugate momentum operator $\hat{\mathfrak{S}}_z = -i\partial_{\varphi_0}$, we can obtain the relation shown below

$$\begin{aligned} \hat{\mathfrak{S}}_z|s\rangle = s|s\rangle, \hat{\varphi}_0|\varphi_0\rangle = \varphi_0|\varphi_0\rangle, \\ e^{\pm i\hat{\varphi}_0}|s\rangle = |s \pm 1\rangle, \left[\hat{\varphi}_0, \hat{\mathfrak{S}}_z\right] = i. \end{aligned} \tag{33}$$

According to the preceding analysis, we can obtain the Hamiltonian of $\mathfrak{S}_z$ qubits

$$\hat{\mathcal{H}}_{\mathfrak{S}_z} = \bar{\bar{\kappa}}_z \hat{\mathfrak{S}}_z^2 - \bar{\bar{h}}_z \hat{\mathfrak{S}}_z - \bar{\bar{\varepsilon}}_z \cos\hat{\varphi}_0. \tag{34}$$

The eigenenergy and eigenstate of the $\mathfrak{S}_z$ qubit can be calculated by solving the Schrödinger equation as follows

$$\hat{\mathcal{H}}_{\mathfrak{S}_z}\Psi_s(\varphi_0) = \mathfrak{E}_s \Psi_s(\varphi_0) \tag{35}$$

with the state $\Psi_s(\varphi_0) = \langle\varphi_0|s\rangle$ and $\Psi_s(\varphi_0) = \Psi_s(\varphi_0 + 2\pi)$. Calculating Eq. (35), we can obtain the damped Mathieu equation [9, 10]

$$\left[\partial_{\varphi_0}^2 - i\widetilde{h}\partial_{\varphi_0} + \frac{\mathfrak{E}_s}{\bar{\bar{\kappa}}_z} + \frac{\bar{\bar{\varepsilon}}_z}{\bar{\bar{\kappa}}_z}\cos\varphi_0\right]\Psi_s(\varphi_0) = 0 \tag{36}$$

with $\widetilde{h} \equiv \bar{\bar{h}}_z/\bar{\bar{\kappa}}_z$. Using the Liouville transformation $\Psi_s(\varphi_0) = \psi_s(\varphi_0)\exp(i\widetilde{h}\varphi_0/2)$ [10], the damping term can be eliminated to obtain the standard Mathieu equation

$$\partial_{\varphi_0}^2 \psi_s(\varphi_0) + \left[\alpha_x + q_x\cos\varphi_0\right]\psi_s(\varphi_0) = 0, \tag{37}$$

where $\alpha_x = \widetilde{h}^2/4 + \mathfrak{E}_s/\bar{\bar{\kappa}}_z$ and $q_x = \bar{\bar{\varepsilon}}_z/\bar{\bar{\kappa}}_z$. Then the eigenvalues and eigenfunctions of Eq. (37) can be written as

$$\begin{aligned} \alpha_x &= \frac{\mathfrak{M}_A(\mathfrak{N}, -2q_x)}{4}, \\ \psi_s(\varphi_0) &= \sum_{j=C/S} \mathfrak{C}_j \mathfrak{M}_j\left(4\alpha_x, -2q_x, \varphi_0/2\right), \end{aligned} \tag{38}$$

where $\mathfrak{M}_S$ and $\mathfrak{M}_C$ represent the odd and even solutions, respectively. $\mathfrak{N}$ is the characteristic index. As illustrated in manuscript, the energy level of the $\mathfrak{S}_z$ qubit is inhomogeneous, so we truncate the Hilbert space to the subspace $\{|0\rangle, |1\rangle\}$, in which case the $\mathfrak{S}_z$ qubit Hamiltonian can be written as

$$\hat{H}_{\text{Sky}} = \frac{\mathcal{A}_0}{2}\hat{\sigma}_z^{\text{sub}} - \frac{\mathcal{B}_0}{2}\hat{\sigma}_x^{\text{sub}}, \tag{39}$$

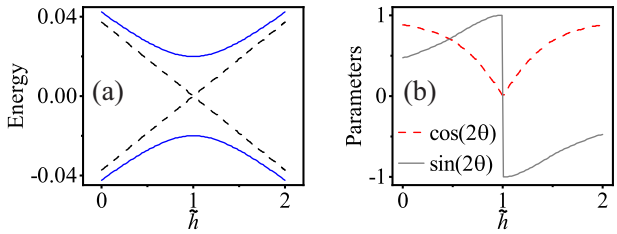

FIG. S3. (a) The energy levels of the $\mathfrak{S}_z$ qubit as a function of the applied magnetic field. Given the same conditions as (a), (b) shows the variation of $\cos(2\theta)$ and $\sin(2\theta)$ and demonstrates that $\sin(2\theta) \sim 1$ and $\cos(2\theta) \sim 0$ can be obtained near the degeneracy point.

where $\mathcal{A}_0 \equiv \bar{\bar{\kappa}}_z - \bar{\bar{h}}_z$, $\mathcal{B}_0 \equiv \bar{\bar{\varepsilon}}_z$, and the Pauli operators are defined as $\hat{\sigma}_z^{\text{sub}} \equiv |1\rangle\langle 1| - |0\rangle\langle 0|$ and $\hat{\sigma}_x^{\text{sub}} \equiv |1\rangle\langle 0| + |0\rangle\langle 1|$. Diagonalizing $\hat{H}_{\text{Sky}}$ obtains the basis vectors $|\psi_+\rangle = \cos\theta|1\rangle - \sin\theta|0\rangle$ and $|\psi_-\rangle = \sin\theta|1\rangle + \cos\theta|0\rangle$, as well as their corresponding eigenenergies $\mathcal{E}_\pm = \pm 1/2\sqrt{\mathcal{A}_0^2 + \mathcal{B}_0^2}$, where $\tan(2\theta) = \mathcal{B}_0/\mathcal{A}_0$. The energy levels of the skyrmion qubits as a function of the applied magnetic field are depicted in FIG. S3(a). The dashed line depicts the case where the applied electric field gradient $E = 0$, and it can be observed that the energy levels of the $\mathfrak{S}_z$ qubit are degenerate. The $\mathfrak{S}_z$ qubit's energy levels are nondegenerate when an external electric field gradient is introduced (blue solid line). The energy level gap is modulated by the applied electric field around the degeneracy point.

2. *Collective coordinate quantization*

This part will show the primary process of the collective coordinate quantization method. The partition function of the skyrmion model investigated here can be represented as

$$\mathcal{Z} = \int \mathcal{D}\boldsymbol{s} \exp\left[i\mathcal{S}\left(\boldsymbol{s}, \dot{\boldsymbol{s}}\right)\right], \tag{40}$$

where the action is given by $S = \int dt\mathcal{L}$. The system's Lagrangian is

$$\mathcal{L} = \bar{S} \int d\boldsymbol{r}\left[\mathfrak{A}(\boldsymbol{s}) \cdot \dot{\boldsymbol{s}} - \mathcal{F}\right], \tag{41}$$

where $\mathfrak{A}(\boldsymbol{s}) = \{[1 - \widetilde{e}_\Phi \cdot (e_\Phi \times \boldsymbol{s})]/(\widetilde{e}_\Phi \cdot \boldsymbol{s})\} e_\Phi$ is the gauge potential with $\widetilde{e}_\Phi = (\cos\Phi, \sin\Phi, 0)$ and $e_\Phi = (-\sin\Phi, \cos\Phi, 0)$. $\mathcal{F}$ represents the energy density functional, defined as

$$\mathcal{F} = -\frac{\mathcal{J}_1}{2}(\nabla_{\widetilde{\boldsymbol{r}}}\boldsymbol{s})^2 + \frac{\mathcal{J}_2 a^2}{2}(\nabla^2_{\widetilde{\boldsymbol{r}}}\boldsymbol{s})^2 - \frac{H}{a^2}s_z + \frac{K}{a^2}s_z^2. \tag{42}$$

It is worth noting that $\mathfrak{A}(\boldsymbol{s}) \cdot \boldsymbol{s} = (1 - \cos\Theta)\dot{\Phi}$. As the global symmetry of the model $\mathcal{F}$ is unbroken, we can obtain $\boldsymbol{s} \to \mathcal{M}(\varphi_0)\boldsymbol{s}$ with

$$\mathcal{M}(\varphi_0) = \begin{pmatrix} \cos\varphi_0 & -\sin\varphi_0 & 0 \\ \sin\varphi_0 & \cos\varphi_0 & 0 \\ 0 & 0 & 1 \end{pmatrix}. \tag{43}$$

For convenience, we introduce $\boldsymbol{n} = \sqrt{1 - \cos\Theta}\boldsymbol{s}/\sin\Theta$. The gauge potential is thus determined to be $\mathfrak{A}(\boldsymbol{n}) = \partial_\Phi \boldsymbol{n}$. To eliminate the zero mode, we introduce the δ constraint according to standard collective coordinate quantization, and the δ constraint is defined as [8]

$$\int \mathcal{D}\varphi_0 \mathcal{D}\mathfrak{S}_z J_{\varphi_0} J_{\mathfrak{S}_z} \delta(F_1)\delta(F_2) = 1, \tag{44}$$

where

$$\begin{aligned} F_1 &= \int d\boldsymbol{r}\mathfrak{A}(\boldsymbol{n}_0) \cdot (\widetilde{\boldsymbol{n}} - \boldsymbol{n}_0), \\ F_2 &= \frac{1}{\Lambda}\int d\boldsymbol{r}\mathfrak{A}(\boldsymbol{n}_0) \cdot \left[\widetilde{\mathfrak{A}}(\boldsymbol{n}) - \mathfrak{A}(\boldsymbol{n}_0)\right], \\ J_{\varphi_0} &= \frac{\delta F_1}{\delta\varphi_0}, \; J_{\mathfrak{S}_z} = \frac{\delta F_2}{\delta\mathfrak{S}_z}. \end{aligned} \tag{45}$$

The Jacobians of the transformation are J_{φ_0} and $J_{\mathfrak{S}_z}$. Here, we assume that the skyrmion consists of its classical part and quantum fluctuation components, i.e. $\boldsymbol{n} = \widetilde{\boldsymbol{n}}_0 + \widetilde{\boldsymbol{\gamma}}$ and $\mathfrak{A}(\boldsymbol{n}) = c\widetilde{\mathfrak{A}}(\boldsymbol{n}_0) + \widetilde{\boldsymbol{\zeta}}$. The presence of parameter c ensures that the aforementioned transformation is canonical, meaning that the transformed Wess-Zumino (WZ) term maintains its original form. The momentum conservation constraint $P - \mathfrak{S}_z = F_2$ allows us to derive

$$c = \frac{\mathfrak{S}_z - \int d\boldsymbol{r}\widetilde{\boldsymbol{\zeta}} \cdot \partial_\phi \boldsymbol{n}}{\int d\boldsymbol{r}\widetilde{\mathfrak{A}}(\boldsymbol{n}_0) \cdot \partial_\phi \boldsymbol{n}}. \tag{46}$$

Thus $\int dtd\boldsymbol{r}\mathfrak{A}(\boldsymbol{n}) \cdot \dot{\boldsymbol{n}} = \int dt\mathfrak{S}_z\dot{\varphi}_0 + \int dtd\boldsymbol{r}\boldsymbol{\zeta} \cdot \dot{\boldsymbol{\gamma}}$ can be deduced, showing that the WZ term maintains the canonical form under the transformation mentioned above.

In the following, the transformation of the energy functional $\mathcal{F}$ is analyzed. For convenience, we introduce the transformation

$$\begin{aligned} \widetilde{\Pi}(\boldsymbol{r}, t) &= \frac{\mathfrak{S}_z - \int d\boldsymbol{r}\eta(\boldsymbol{r}, \boldsymbol{t})\partial_\phi \Phi(\boldsymbol{r}, t)}{\Lambda}\widetilde{\Pi}_0(\boldsymbol{r}, t) + \eta(\boldsymbol{r}, t), \\ \Phi(\boldsymbol{r}, t) &= \Phi_0\left[\boldsymbol{r}, \varphi_0(t)\right] + \xi(\boldsymbol{r}, t). \end{aligned} \tag{47}$$

The transformation preserves the canonical form of the WZ term, which is $\int d\boldsymbol{r}\widetilde{\Pi}\dot{\Phi} = \mathfrak{S}_z\dot{\varphi}_0 + \int d\boldsymbol{r}\eta\dot{\xi}$. The Hamiltonian of skyrmion qubits can therefore be simplified as

$$\mathcal{H}_{\mathfrak{S}_z} = \bar{\bar{\kappa}}_z\mathfrak{S}_z^2 - \bar{\bar{h}}_z\mathfrak{S}_z - \bar{\bar{\varepsilon}}_z\cos\varphi_0. \tag{48}$$

III. COHERENT COUPLING BETWEEN THE YIG SPHERE AND THE SKYRMION

A. The magnetic field of the YIG sphere

Here the cylindrical coordinate system is established with the center of the skyrmion as the coordinate origin, and the skyrmion lies in the xy plane. Then the coordinates of any point on the skyrmion can be expressed as $(\widetilde{\rho}\cos\phi, \widetilde{\rho}\sin\phi, 0)$. The center of the YIG sphere lies on the z axis, directly above the skyrmion, and its coordinates are $(0, 0, h_K)$. The position vector from the center of the YIG sphere to any location on the skyrmion plane is then $\boldsymbol{r} = (\widetilde{\rho}\cos\phi, \widetilde{\rho}\sin\phi, -h_K)$. In classical electrodynamics, the magnetic field generated by a magnetic sphere at position $\boldsymbol{r}$ can be described by the magnetic dipole model, which is given by

$$\boldsymbol{B} = \frac{\mu_0}{4\pi}\left[\frac{3\boldsymbol{r}(\boldsymbol{\mu}\cdot\boldsymbol{r})}{r^5} - \frac{\boldsymbol{\mu}}{r^3}\right], \tag{49}$$

where $\boldsymbol{\mu}$ is the magnetic moment. The YIG sphere's magnetic moment can be written as $\boldsymbol{\mu} = \boldsymbol{M}4\pi R_K^3/3$, and Eq. (49) can therefore be simplified as

$$\boldsymbol{B} = \frac{\mu_0 R_K^3}{3}\left[\frac{3\boldsymbol{r}(\boldsymbol{M}\cdot\boldsymbol{r})}{r^5} - \frac{\boldsymbol{M}}{r^3}\right], \tag{50}$$

where $\boldsymbol{M}$ is the YIG sphere's magnetization. The magnetization $\boldsymbol{M}$ can be quantized as $\hat{\boldsymbol{M}} = M_K[\widetilde{\boldsymbol{m}}_K\hat{s}_K + \widetilde{\boldsymbol{m}}_K^*\hat{s}_K^\dagger]$ based on the analysis in Sec. I. Here, the Kittel mode, whose mode function is $\widetilde{\boldsymbol{m}}_K = \hat{\boldsymbol{e}}_z + i\hat{\boldsymbol{e}}_x$, is the primary focus of our discussion. Then the quantized magnetic field can be represented as

$$\hat{\boldsymbol{B}}_{r^5} = \frac{\mu_0 R_K^3}{3}\left\{\frac{3}{r^5}M_K\left[\widetilde{\rho}\cos\phi i\left(\hat{s}_K - \hat{s}_K^\dagger\right) - h_K\left(\hat{s}_K + \hat{s}_K^\dagger\right)\right](\widetilde{\rho}\cos\phi, \widetilde{\rho}\sin\phi, -h_K)\right\}, \tag{51a}$$

$$\hat{\boldsymbol{B}}_{r^3} = \frac{\mu_0 R_K^3}{3}\left\{-\frac{1}{r^3}M_K\left[i\left(\hat{s}_K - \hat{s}_K^\dagger\right), 0, \left(\hat{s}_K + \hat{s}_K^\dagger\right)\right]\right\}, \tag{51b}$$

$$\hat{\boldsymbol{B}} = \hat{\boldsymbol{B}}_{r^5} + \hat{\boldsymbol{B}}_{r^3}. \tag{51c}$$

By writing the magnetic field components, one obtains

$$\hat{B}_x = \frac{\mu_0 R_K^3}{3}\left\{\frac{3M_K}{r^5}\left[i\widetilde{\rho}\cos\phi\left(\hat{s}_K - \hat{s}_K^\dagger\right) - h_K\left(\hat{s}_K + \hat{s}_K^\dagger\right)\right]\widetilde{\rho}\cos\phi - \frac{iM_K}{r^3}\left(\hat{s}_K - \hat{s}_K^\dagger\right)\right\}, \tag{52a}$$

$$\hat{B}_y = \frac{\mu_0 R_K^3}{3}\left\{\frac{3M_K}{r^5}\left[i\widetilde{\rho}\cos\phi\left(\hat{s}_K-\hat{s}_K^\dagger\right)-h_K\left(\hat{s}_K+\hat{s}_K^\dagger\right)\right]\widetilde{\rho}\sin\phi\right\}, \tag{52b}$$

$$\hat{B}_z = \frac{\mu_0 R_K^3}{3}\left\{-\frac{3M_K h_K}{r^5}\left[i\widetilde{\rho}\cos\phi\left(\hat{s}_K-\hat{s}_K^\dagger\right)-h_K\left(\hat{s}_K+\hat{s}_K^\dagger\right)\right]-\frac{M_K}{r^3}\left(\hat{s}_K+\hat{s}_K^\dagger\right)\right\}. \tag{52c}$$

B. The interaction Hamiltonian

The interaction between the magnetic field $\hat{\boldsymbol{B}}$ generated by the YIG sphere and the spin $\boldsymbol{s}_i$ at the position $\boldsymbol{r}_i$ of the skyrmion can be described by the Hamiltonian

$$\hat{H}_{\mathrm{KS}} = -g\mu_B\bar{S}\sum_i \hat{\boldsymbol{B}}\cdot\boldsymbol{s}_i. \tag{53}$$

Utilizing the continuity condition, the summation in the Hamiltonian Eq. (53) can be reduced to an integral, i.e., the interaction Hamiltonian can be written as

$$\hat{H}_{\mathrm{KS}} = -\frac{g\mu_B\bar{S}}{a^2}\int d\widetilde{\boldsymbol{r}}\hat{\boldsymbol{B}}\cdot\boldsymbol{s}, \tag{54}$$

where a is the lattice spacing. Writing the interaction Hamiltonian in the component form yields

$$\hat{H}_{\mathrm{KS}} = -\frac{g\mu_B\bar{S}}{a^2}\int d\widetilde{x}d\widetilde{y}\left(\hat{B}_x\cdot s_x+\hat{B}_y\cdot s_y+\hat{B}_z\cdot s_z\right). \tag{55}$$

The coupling of the x-direction magnetic field and the skyrmion can be described by

$$\begin{aligned}\hat{H}_{\mathrm{KS}}^x = &-\frac{g\mu_B\bar{S}}{a^2}\\ &\times\int d\widetilde{x}d\widetilde{y}\frac{\mu_0 R_K^3}{3}\left\{\frac{3M_K}{r^5}\left[i\widetilde{\rho}\cos\phi\left(\hat{s}_K-\hat{s}_K^\dagger\right)-h_K\left(\hat{s}_K+\hat{s}_K^\dagger\right)\right]\widetilde{\rho}\cos\phi-\frac{iM_K}{r^3}\left(\hat{s}_K-\hat{s}_K^\dagger\right)\right\}\cdot\sin\Theta_0\cos\Phi,\end{aligned} \tag{56}$$

where $\Phi=\phi+\varphi_0$. Making the integral in Eq. (56) dimensionless, we can obtain

$$\begin{aligned}\hat{H}_{\mathrm{KS}}^x = &-\frac{g\mu_B\bar{S}}{a^3}\\ &\times\int\frac{\mu_0 R_K^3}{3}\left\{\frac{3M_K}{r^5}\left[i\rho\cos\phi\left(\hat{s}_K-\hat{s}_K^\dagger\right)-h_K\left(\hat{s}_K+\hat{s}_K^\dagger\right)\right]\rho\cos\phi-\frac{iM_K}{r^3}\left(\hat{s}_K-\hat{s}_K^\dagger\right)\right\}\\ &\cdot\sin\Theta_0\cos\Phi dxdy,\end{aligned} \tag{57}$$

Transforming the above integral Eq. (57) to polar coordinates

$$\begin{aligned}\hat{H}_{\mathrm{KS}}^x = &-\frac{g\mu_B\bar{S}}{a^3}\\ &\times\int\frac{\mu_0 R_K^3}{3}\left\{\frac{3M_K}{r^5}\left[i\rho\cos\phi\left(\hat{s}_K-\hat{s}_K^\dagger\right)-h_K\left(\hat{s}_K+\hat{s}_K^\dagger\right)\right]\rho\cos\phi-\frac{iM_K}{r^3}\left(\hat{s}_K-\hat{s}_K^\dagger\right)\right\}\\ &\cdot\sin\Theta_0\cos\left(\phi+\varphi_0\right)\rho d\rho d\rho d\phi,\end{aligned} \tag{58}$$

we can find that the integral over ρ and ϕ are completely independent of one another. Considering first the integration over ϕ and dropping the term whose integration is zero, Eq. (58) can be simplified to

$$\hat{H}_{\mathrm{KS}}^x = -\frac{g\mu_B\bar{S}}{a^3}\int\rho d\rho d\rho d\phi\frac{\mu_0 R_K^3}{3}\left\{\frac{3M_K}{r^5}\left[-h_K\left(\hat{s}_K+\hat{s}_K^\dagger\right)\right]\right\}\rho\sin\Theta_0\cos^2\phi\cos\varphi_0, \tag{59}$$

For the second term of Eq. (55), the Hamiltonian of the interaction between the y-direction magnetic field and the skyrmion can be obtained by the same calculation

$$\hat{H}_{\mathrm{KS}}^y = -\frac{g\mu_B\bar{S}}{a^3}\int\rho d\rho d\rho d\phi\frac{\mu_0 R_K^3}{3}\left\{\frac{3M_K}{r^5}\left[-h_K\left(\hat{s}_K+\hat{s}_K^\dagger\right)\right]\right\}\rho\sin\Theta_0\sin^2\phi\cos\varphi_0. \tag{60}$$

We define transverse coupling

$$\hat{H}_{\mathrm{KS}}^{xy}=\hat{H}_{\mathrm{KS}}^{x}+\hat{H}_{\mathrm{KS}}^{y}. \tag{61}$$

Substituting Eq. (59) and Eq. (60) into Eq. (61) results in

$$\hat{H}_{\mathrm{KS}}^{xy}=\frac{2\pi g\mu_B\bar{S}\mu_0R_K^3M_K}{a^3}\left(\hat{s}_K+\hat{s}_K^{\dagger}\right)\cos\varphi_0\int\rho d\rho\frac{\rho h_K\sin\Theta_0}{\left(\rho^2+h_K^2\right)^{5/2}}. \tag{62}$$

Define the transverse coupling strength

$$\lambda_{\mathrm{KS}}^{xy}=\frac{2\pi g\mu_B\bar{S}\mu_0R_K^3M_K}{a^3}\int\rho d\rho\frac{\rho h_K\sin\Theta_0}{\left(\rho^2+h_K^2\right)^{5/2}}. \tag{63}$$

Then Eq. (62) can be reduced to

$$\hat{H}_{\mathrm{KS}}^{xy}=\lambda_{\mathrm{KS}}^{xy}\left(\hat{s}_K+\hat{s}_K^{\dagger}\right)\cos\hat{\varphi}_0. \tag{64}$$

Here the operator $\hat{\varphi}_0$ has been used. In the following we calculate the third term in Eq. (55)

$$\hat{H}_{\mathrm{KS}}^{z}=-\frac{g\mu_B\bar{S}}{a^2}\int d\widetilde{x}d\widetilde{y}\left(\hat{B}_z\cdot s_z\right). \tag{65}$$

Substituting Eq. (52c) into Eq. (65), one can get

$$\hat{H}_{\mathrm{KS}}^{z}=-\frac{g\mu_B\bar{S}}{a^2}\frac{\mu_0R_K^3}{3}M_K\left(\hat{s}_K+\hat{s}_K^{\dagger}\right)\int d\widetilde{x}d\widetilde{y}\left\{\frac{3h_K^2}{\left(\widetilde{x}^2+\widetilde{y}^2+h_K^2\right)^{5/2}}-\frac{1}{\left(\widetilde{x}^2+\widetilde{y}^2+h_K^2\right)^{3/2}}\right\}\cos\Theta, \tag{66}$$

where the term with zero integration over ϕ has been ignored, as in the calculation of the transverse coupling $\hat{H}_{\mathrm{KS}}^{xy}$. Dimensionlessizing the integral Eq. (66), one can get

$$\hat{H}_{\mathrm{KS}}^{z}=-\frac{g\mu_B\bar{S}}{a^3}\frac{\mu_0R_K^3}{3}M_K\left(\hat{s}_K+\hat{s}_K^{\dagger}\right)\int dxdy\left\{\frac{3h_K^2}{\left(x^2+y^2+h_K^2\right)^{5/2}}-\frac{1}{\left(x^2+y^2+h_K^2\right)^{3/2}}\right\}\Pi, \tag{67}$$

where $\Pi=\cos\Theta$. With $\Pi=1-\widetilde{\Pi}$ and Eq. (30), Eq. (67) can be reduced to

$$\hat{H}_{\mathrm{KS}}^{z}=\frac{g\mu_B\bar{S}}{a^3}\frac{\mu_0R_K^3}{3}M_K\left(\hat{s}_K+\hat{s}_K^{\dagger}\right)\frac{\hat{\mathfrak{S}}_z}{\Lambda}\int dxdy\left\{\frac{3h_K^2}{\left(x^2+y^2+h_K^2\right)^{5/2}}-\frac{1}{\left(x^2+y^2+h_K^2\right)^{3/2}}\right\}\left(1-\cos\Theta_0\right). \tag{68}$$

Here we discount the term containing η, which describes the associated magnon fluctuations. Expressing the Eq. (68) using polar coordinates yields

$$\hat{H}_{\mathrm{KS}}^{z}=\frac{g\mu_B\bar{S}}{a^3}\frac{\mu_0R_K^3}{3}M_K\left(\hat{s}_K+\hat{s}_K^{\dagger}\right)\frac{\hat{\mathfrak{S}}_z}{\Lambda}\int\rho d\rho d\phi\left\{\frac{3h_K^2}{\left(\rho^2+h_K^2\right)^{5/2}}-\frac{1}{\left(\rho^2+h_K^2\right)^{3/2}}\right\}\left(1-\cos\Theta_0\right). \tag{69}$$

Defining the longitudinal coupling strength

$$\lambda_{\mathrm{KS}}=\frac{\pi g\mu_B\bar{S}\mu_0}{3a^3\Lambda}\sqrt{\frac{3\hbar\gamma_eM_s}{2\pi}}R_K^{3/2}\mathcal{F}(\rho) \tag{70}$$

and the dimensionless integral

$$\mathcal{F}(\rho)=\int d\rho\frac{2h_K^2\rho-\rho^3}{\left(\rho^2+h_K^2\right)^{5/2}}\left(1-\cos\Theta_0\right), \tag{71}$$

with $h_K=R_K+d_K$, the Hamiltonian of the longitudinal coupling is

$$\hat{H}_{\mathrm{KS}}^{z}=\lambda_{\mathrm{KS}}\left(\hat{s}_K+\hat{s}_K^{\dagger}\right)\hat{\mathfrak{S}}_z. \tag{72}$$

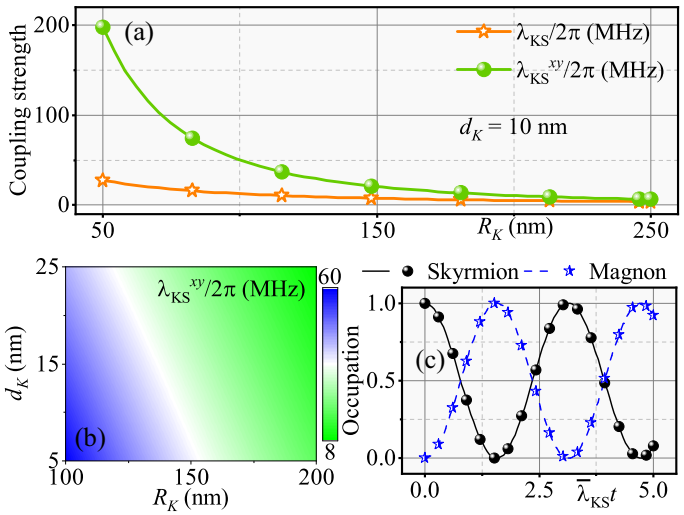

FIG. S4. (a) Comparison of transverse $\hat{H}_{\rm KS}^{xy}$ and longitudinal $\hat{H}_{\rm KS}^{z}$ coupling. (b) Variation of transverse coupling strength $\lambda_{\rm KS}^{xy}$ with radius R_K and distance d_K. (c) Dynamical evolution of systems with and without transverse coupling $\hat{H}_{\rm KS}^{xy}$. Black and blue represent the skyrmion and magnon, respectively. The scattered dots and curves represent the dynamical evolution in the presence and absence of transverse coupling $\hat{H}_{\rm KS}^{xy}$, respectively. The parameters are $\gamma_{\rm Sky} = \gamma_{\rm K} = 0$, $\bar{\lambda}_{\rm KS}^{xy} = 4\bar{\lambda}_{\rm KS}$, and $\omega_q = \omega_K = 1000\bar{\lambda}_{\rm KS}$.

The total Hamiltonian for the interaction of the YIG sphere and skyrmion is

$$\hat{H}_{\rm KS} = \hat{H}_{\rm KS}^{xy} + \hat{H}_{\rm KS}^{z}. \tag{73}$$

The parameters involved in the coupling strength Eq. (63) and Eq. (70) are zero-point magnetization $M_K = \sqrt{\hbar\gamma_e M_s/(2V_K)}$, gyromagnetic ratio γ_e, saturation magnetization M_s, volume of the YIG sphere V_K, and $\Lambda = \int d\boldsymbol{r}(1-\cos\Theta_0)$. As shown in Fig. S4(a), it can be found that when the radius of the YIG sphere is small, the transverse coupling is larger than the longitudinal coupling, but as the radius of the YIG sphere increases, the two gradually tend to be the same. The variation of the transverse coupling strength and the longitudinal coupling strength with d_K and R_K are shown in Fig. S4(b) and in Fig. 2(a) of the main text, respectively. Taking the parameters $d_K = 10$ nm and $R_K = 100$ nm, we can get $\lambda_{\rm KS}/2\pi = 12.7$ MHz and $\lambda_{\rm KS}^{xy}/2\pi = 50.1$ MHz.

C. Approximate analysis of the coupling strength $\lambda_{\rm KS}$

In Eq. (70), the inclusion of the integral $\mathcal{F}(\rho)$ prohibits us from displaying the coupling strength's dependency on R_K and d_K. In this section, we will provide an approximation for the coupling strength $\lambda_{\rm KS}$ that is consistent with the analytical results. For analytical purposes, we define

$$f(\rho) = \frac{2h_K^2\rho - \rho^3}{\left(\rho^2 + h_K^2\right)^{5/2}}\left(1-\cos\Theta_0\right). \tag{74}$$

Directly solving for the original function of $f(\rho)$ is extremely challenging. Furthermore, the presence of the trigonometric function $\cos\Theta_0$ prohibits us from approximating its solution using a series expansion. However, by evaluating the series expansion of the function $f(\rho)$ near 0, we find that applying a constant correction factor yields a fairly good approximation to the precise solution. Expanding the function at 0 to order 1 results in

$$f^{(1)}(\rho) \approx \frac{4\rho}{h_K^3}. \tag{75}$$

Figure S5(a) shows that the approximation function $f^{(1)}(\rho)$ can only estimate $f(\rho)$ up to the maximum, beyond which it is not adequately approximated due to the existence of trigonometric functions. However, we find that in the range of parameters we are interested in, the area of integration of $f^{(1)}(\rho)$ equals $1/\Upsilon = 37.5$ times the area of integration of

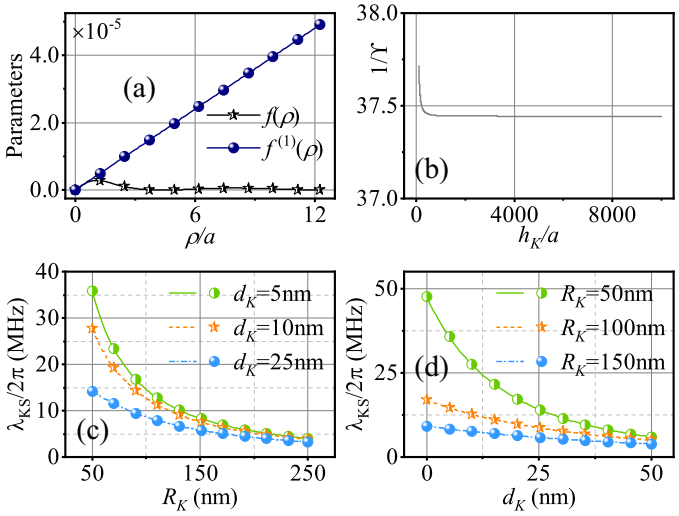

FIG. S5. (a) The functions $f^{(1)}(\rho)$ and $f(\rho)$. (b) The variation of the correction factor $1/\Upsilon$ with the parameter h_K that we are interested in. (c, d) The longitudinal coupling strength as a function of R_K and d_K. The curves and scatters correspond to the results of the precise and approximate forms of coupling strength, $\lambda_{\rm KS}$ and $\lambda_{\rm KS}^{\rm App}$, respectively.

$f(\rho)$, and that Υ is nearly constant when the values are altered [Fig. S5(b)]. With the introduction of the correction factor Υ, the integral $\mathcal{F}(\rho)$ can be approximated as

$$\mathcal{F}(\rho) \approx \int d\rho \Upsilon \frac{4\rho}{h_K^3} = \Upsilon \frac{2\mathcal{R}^2}{h_K^3}. \tag{76}$$

The coupling strength can then be reduced as follows:

$$\lambda_{\rm KS}^{\rm App} = \mathcal{K}_0 \frac{2\mathcal{R}^2 R_K^{3/2}}{(d_K + R_K)^3} \tag{77}$$

with constant

$$\mathcal{K}_0 = \Upsilon \frac{\pi g \mu_B \bar{S} \mu_0}{3a^3 \Lambda} \sqrt{\frac{3\hbar\gamma_e M_s}{2\pi}}. \tag{78}$$

Figures S5(c) and (d) depict the variation of coupling strength with R_K and d_K using the precise solution (70) and the approximate solution (77), respectively. The results of the computations with Eqs. (70) and (77) are in good agreement. According to the approximate solution $\lambda_{\rm KS}^{\rm App}$, the coupling strength decreases polynomially rather than exponentially with R_K and d_K.

D. The Hamiltonian of the hybrid system

Firstly, in the subspace $\{|0\rangle, |1\rangle\}$, the interaction Hamiltonian can be expanded as

$$\hat{H}_{\rm KS} = \frac{\lambda_{\rm KS}^{xy}}{2}\left(\hat{s}_K + \hat{s}_K^\dagger\right)\hat{\sigma}_x^{\rm sub} + \frac{\lambda_{\rm KS}}{2}\left(\hat{s}_K + \hat{s}_K^\dagger\right)\hat{\sigma}_z^{\rm sub}, \tag{79}$$

Exploiting the eigenstates $|\psi_+\rangle = \cos\theta|1\rangle - \sin\theta|0\rangle$ and $|\psi_-\rangle = \sin\theta|1\rangle + \cos\theta|0\rangle$ obtained by diagonalizing $\hat{H}_{\rm Sky}$ in the main text, the interaction Hamiltonian can be reduced to

$$\hat{H}_{\rm KS} = \frac{\lambda_{\rm KS}^{xy}}{2}(\hat{s}_K + \hat{s}_K^\dagger)[-\sin(2\theta)\hat{\sigma}_z + \cos(2\theta)\hat{\sigma}_x] + \frac{\lambda_{\rm KS}}{2}(\hat{s}_K + \hat{s}_K^\dagger)[\cos(2\theta)\hat{\sigma}_z + \sin(2\theta)\hat{\sigma}_x] \tag{80}$$

with the Pauli operators $\hat{\sigma}_z = |\psi_+\rangle\langle\psi_+| - |\psi_-\rangle\langle\psi_-|$, $\hat{\sigma}_+ = |\psi_+\rangle\langle\psi_-|$, $\hat{\sigma}_- = |\psi_-\rangle\langle\psi_+|$, and $\hat{\sigma}_x = \hat{\sigma}_+ + \hat{\sigma}_-$. As shown in Fig. S3(b), when the $\mathfrak{S}_z$ qubit works near the degeneracy point, we can get $\cos(2\theta) \sim 0$ and $\sin(2\theta) \sim 1$. In this case, Eq. (80) is denoted as

$$\hat{H}_{\rm KS} = -\bar{\lambda}_{\rm KS}^{xy}(\hat{s}_K + \hat{s}_K^\dagger)\hat{\sigma}_z + \bar{\lambda}_{\rm KS}(\hat{s}_K + \hat{s}_K^\dagger)\hat{\sigma}_x, \tag{81}$$

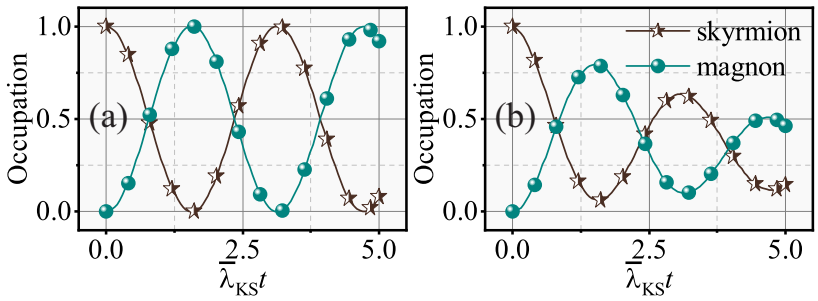

FIG. S6. With the parameters $\omega_q = \omega_K = 1000\bar{\lambda}_{\rm KS}$ and $\gamma_K = \gamma_{\rm Sky} = 0.1\bar{\lambda}_{\rm KS}$, (a, b) show the dynamical evolution of the hybrid quantum system in ideal conditions (a) and (b) in the presence of dissipation, respectively.

where $\bar{\lambda}^{xy}_{\rm KS} = \lambda^{xy}_{\rm KS}\sin(2\theta)/2$ and $\bar{\lambda}_{\rm KS} = \lambda_{\rm KS}\sin(2\theta)/2$. Then the hybrid quantum system's Hamiltonian is given by

$$\hat{H}_{\rm TKS} = \frac{\omega_q}{2}\hat{\sigma}_z + \omega_K\hat{s}^\dagger_K\hat{s}_K + \bar{\lambda}_{\rm KS}\left(\hat{s}_K + \hat{s}^\dagger_K\right)\hat{\sigma}_x - \bar{\lambda}^{xy}_{\rm KS}(\hat{s}_K + \hat{s}^\dagger_K)\hat{\sigma}_z. \tag{82}$$

It is worth noting that the coupling $\lambda^{xy}_{\rm KS}$ does not cause a transition between energy levels, but only a shift in the qubit energy level. We can further write it as $[\omega_q/2 - \bar{\lambda}^{xy}_{\rm KS}(\hat{s}_K + \hat{s}^\dagger_K)]\hat{\sigma}_z$, and we can find that the magnitude of the energy level shift is only on the order of megahertz ($\lambda^{xy}_{\rm KS} \approx 50.1$ MHz), which is much smaller than the hybrid system's gigahertz resonance frequency ($\omega_q \approx \omega_K \approx 9.8$ GHz), so its effect can be neglected. The dynamical evolution with and without the coupling $\hat{H}^{xy}_{\rm KS}$ is shown in Fig. S4(c). It demonstrates that it is reasonable to ignore the coupling $\hat{H}^{xy}_{\rm KS}$. By transforming equation (82) into the interaction picture, we can obtain

$$\hat{H}_{\rm TKS} = \bar{\lambda}_{\rm KS}\left(\hat{s}_K\hat{\sigma}_+ + \hat{s}^\dagger_K\hat{\sigma}_-\right) + \bar{\lambda}_{\rm KS}\left(\hat{s}_K\hat{\sigma}_- e^{-i2\omega_q t} + \hat{s}^\dagger_K\hat{\sigma}_+ e^{i2\omega_q t}\right) - \bar{\lambda}^{xy}_{\rm KS}(\hat{s}_K e^{-i\omega_q t} + \hat{s}^\dagger_K e^{i\omega_q t})\hat{\sigma}_z. \tag{83}$$

Here the resonance condition is $\omega_q \approx \omega_K \approx 9.8$ GHz, and then we have $2\omega_q, \omega_q \gg \bar{\lambda}_{\rm KS}, \bar{\lambda}^{xy}_{\rm KS}$. According to the large detuning condition, the terms $\bar{\lambda}_{\rm KS}\left(\hat{s}_K\hat{\sigma}_- e^{-i2\omega_q t} + \hat{s}^\dagger_K\hat{\sigma}_+ e^{i2\omega_q t}\right)$ and $\bar{\lambda}^{xy}_{\rm KS}(\hat{s}_K e^{-i\omega_q t} + \hat{s}^\dagger_K e^{i\omega_q t})\hat{\sigma}_z$ are high-frequency oscillation terms and can be ignored, i.e., the hybrid quantum system can be described by the JC model

$$\hat{H}_{\rm TKS} = \bar{\lambda}_{\rm KS}\left(\hat{s}_K\hat{\sigma}_+ + \hat{s}^\dagger_K\hat{\sigma}_-\right). \tag{84}$$

Figure S4(c) demonstrates that it is reasonable to discard the coupling $\bar{\lambda}^{xy}_{\rm KS}$. Figures S6(a, b) depict the dynamical evolution of the hybrid system without and with dissipations, respectively. Rabi oscillations between the two subsystems can be observed in the dynamical evolution of the hybrid quantum system, where the initial states of the magnon and the skyrmion are in the ground and excited states, respectively.

IV. THE SKYRMION-SKYRMION INTERACTION

A. The direct skyrmion-skyrmion interaction

In this section we estimate the direct interaction strength between two skyrmion qubits, as shown in FIG. S7(a). The strength of the interaction between two spins in vacuum can be calculated by the dipole model

$$\frac{J_{\rm dir}}{2\pi} = \frac{\mu_0\mu_B^2}{\hbar(2\pi)^2(2d_{\rm dip})^3}, \tag{85}$$

where $d_{\rm dip}$ is the distance between two spins. The direct coupling between two skyrmion qubits is achieved through dipole-dipole interactions between the layers, described by

$$H_{\rm dir} = -J_{\rm dir}\bar{S}^2\int d\boldsymbol{r}\boldsymbol{s}_1\cdot\boldsymbol{s}_2. \tag{86}$$

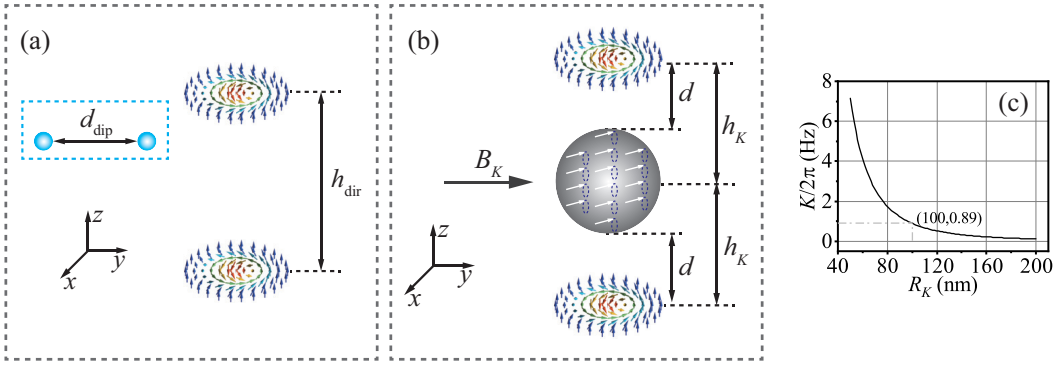

FIG. S7. (a) The setup of direct skyrmion-skyrmion coupling. The insert in the dashed box illustrates the interaction of two dipoles in vacuum. (b) The model of magnon-mediated skyrmion-skyrmion coupling. (c) Variation of the Kerr coefficient with the radius of YIG spheres.

The coupling of the skyrmion qubits between the two layers can be described by the

$$H_{\rm dir} = -J_{\rm dir}\bar{S}^2 \int d\boldsymbol{r} \left[s_x^{(1)} s_x^{(2)} + s_y^{(1)} s_y^{(2)} + + s_z^{(1)} s_z^{(2)} \right]. \tag{87}$$

Then we can get

$$H_{\rm dir} = -J_{\rm dir}\bar{S}^2 \int d\boldsymbol{r} \sin^2\Theta_0 \cos\left(\varphi_0^{(1)} - \varphi_0^{(2)}\right) - \frac{J_{\rm dir}\bar{S}^2}{\Lambda^2} \int d\boldsymbol{r} \left(1-\cos\Theta_0\right)^2 \mathfrak{S}_z^{(1)} \mathfrak{S}_z^{(2)}. \tag{88}$$

After quantization, the Hamiltonian of the direct coupling of skyrmion qubits is given by

$$\hat{H}_{\rm dir} = -\Lambda_{\rm DC} \cos\left(\hat{\varphi}_0^{(1)} - \hat{\varphi_0}^{(2)}\right) - \Lambda_{\rm DC}^z \hat{\mathfrak{S}}_z^{(1)} \hat{\mathfrak{S}}_z^{(2)} \tag{89}$$

with coupling strength $\Lambda_{\rm DC} = 2\pi J_{\rm dir}\bar{S}^2 \int \rho d\rho \sin^2\Theta_0$, $\Lambda_{\rm DC}^z = 2\pi J_{\rm dir}\bar{S}^2/\Lambda^2 \int \rho d\rho (1-\cos\Theta_0)^2$ and $d_{\rm dip} = h_{\rm dir}$. $h_{\rm dir}$ represents the distance between two skyrmion qubits. Here, we can easily verify that $\Lambda_{\rm DC}^z \ll \Lambda_{\rm DC}$ via numerical calculations, then in the later analysis, we mainly focus on the coupling strength $\Lambda_{\rm DC}$.

B. The indirect skyrmion-skyrmion interactions: magnon mediated

When two skyrmion qubits are coupled to the same YIG magnetic sphere [FIG. S7(b)], we can get effective skyrmion-skyrmion interaction by adiabatically eliminating the magnon modes. The skyrmion-magnon-skyrmion hybrid system is described by

$$\hat{H}_{\rm SKS} = \frac{\omega_q}{2}(\hat{\sigma}_z^1 + \hat{\sigma}_z^2) + \omega_K \hat{s}_K^\dagger \hat{s}_K + \bar{\lambda}_{\rm KS}(\hat{s}_K + \hat{s}_K^\dagger)(\hat{\sigma}_x^1 + \hat{\sigma}_x^2). \tag{90}$$

Transforming to a rotating frame with frequency ω_q, we can derive

$$\hat{H}_{\rm SKS} = \Delta \hat{s}_K^\dagger \hat{s}_K + \bar{\lambda}_{\rm KS}\left[\hat{s}_K(\hat{\sigma}_+^1 + \hat{\sigma}_+^2) + \hat{s}_K^\dagger(\hat{\sigma}_-^1 + \hat{\sigma}_-^2)\right], \tag{91}$$

where $\Delta = \omega_K - \omega_q$. In the following we derive the effective Hamiltonian after adiabatic elimination of the magnon modes. With equation $\dot{\hat{A}} = i[\hat{H}, \hat{A}]$ and Eq. (91), the quantum Langevin equations for the system can be written as

$$\dot{\hat{s}}_K = -\left(i\Delta + \frac{\gamma_K}{2}\right)\hat{s}_K - i\bar{\lambda}_{\rm KS}\left(\hat{\sigma}_-^1 + \hat{\sigma}_-^2\right), \tag{92a}$$

$$\dot{\hat{\sigma}}_-^1 = -\frac{\gamma_{\rm Sky}}{2}\hat{\sigma}_-^1 + i\bar{\lambda}_{\rm KS}\hat{s}_K\hat{\sigma}_z^1, \tag{92b}$$

$$\dot{\hat{\sigma}}_-^2 = -\frac{\gamma_{\rm Sky}}{2}\hat{\sigma}_-^2 + i\bar{\lambda}_{\rm KS}\hat{s}_K\hat{\sigma}_z^2, \tag{92c}$$

where γ_{Sky} and γ_K represent the dissipation of skyrmion qubits and magnons, respectively. The formal integral of the equations (92a), (92b), and (92c) can be expressed as

$$\hat{s}_K(t) = \hat{s}_K(0)\exp\left[-\left(i\Delta+\frac{\gamma_K}{2}\right)t\right] + \exp\left[-\left(i\Delta+\frac{\gamma_K}{2}\right)t\right]\int_0^t d\tau\left[-i\bar{\lambda}_{\mathrm{KS}}\left(\hat{\sigma}_-^1(\tau)+\hat{\sigma}_-^2(\tau)\right)\right]\exp\left[\left(i\Delta+\frac{\gamma_K}{2}\right)\tau\right], \tag{93a}$$

$$\hat{\sigma}_-^1(t) = \hat{\sigma}_-^1(0)\exp\left(-\frac{\gamma_{\mathrm{Sky}}}{2}t\right) + \exp\left(-\frac{\gamma_{\mathrm{Sky}}}{2}t\right)\int_0^t d\tau\left[i\bar{\lambda}_{\mathrm{KS}}\hat{s}_K\hat{\sigma}_z^1(\tau)\right]\exp\left(\frac{\gamma_{\mathrm{Sky}}}{2}\tau\right), \tag{93b}$$

$$\hat{\sigma}_-^2(t) = \hat{\sigma}_-^2(0)\exp\left(-\frac{\gamma_{\mathrm{Sky}}}{2}t\right) + \exp\left(-\frac{\gamma_{\mathrm{Sky}}}{2}t\right)\int_0^t d\tau\left[i\bar{\lambda}_{\mathrm{KS}}\hat{s}_K\hat{\sigma}_z^2(\tau)\right]\exp\left(\frac{\gamma_{\mathrm{Sky}}}{2}\tau\right). \tag{93c}$$

Here we consider the case $\Delta, \gamma_K \gg \bar{\lambda}_{\mathrm{KS}}, \gamma_{\mathrm{Sky}}$, that is, the magnon mode and the skyrmion qubit are far from resonance, and the dissipation of the magnon mode is large, indicating that the dynamics of the skyrmion qubits are little affected by the magnon mode, then we can derive

$$\hat{\sigma}_-^1(t) \simeq \hat{\sigma}_-^1(0)\exp\left(-\frac{\gamma_{\mathrm{Sky}}}{2}t\right), \tag{94a}$$

$$\hat{\sigma}_-^2(t) \simeq \hat{\sigma}_-^2(0)\exp\left(-\frac{\gamma_{\mathrm{Sky}}}{2}t\right). \tag{94b}$$

Substituting equations (94a) and (94b) into the integral equation of the magnon mode (93a) yields

$$\hat{s}_K(t) \simeq \frac{-i\bar{\lambda}_{\mathrm{KS}}\hat{\sigma}_-^1(t)}{i\Delta+\gamma_K/2} + \frac{-i\bar{\lambda}_{\mathrm{KS}}\hat{\sigma}_-^2(t)}{i\Delta+\gamma_K/2}. \tag{95}$$

Inserting Eq. (95) into Eq. (92b) and Eq. (92c), we obtain the quantum Langevin equations after eliminating the magnon mode

$$\dot{\hat{\sigma}}_-^1 = \left[i\beta^2\Delta - \frac{\gamma_{\mathrm{Sky}}+\beta^2\gamma_K}{2}\right]\hat{\sigma}_-^1 + i\beta\bar{\lambda}_{\mathrm{KS}}\hat{\sigma}_-^2\hat{\sigma}_z^1, \tag{96a}$$

$$\dot{\hat{\sigma}}_-^2 = \left[i\beta^2\Delta - \frac{\gamma_{\mathrm{Sky}}+\beta^2\gamma_K}{2}\right]\hat{\sigma}_-^2 + i\beta\bar{\lambda}_{\mathrm{KS}}\hat{\sigma}_-^1\hat{\sigma}_z^2, \tag{96b}$$

with $\beta \equiv \bar{\lambda}_{\mathrm{KS}}/\sqrt{\Delta^2+\gamma_K^2/4}$. Here the case $\Delta \gg \gamma_K$ is considered, at which case $\beta \approx \bar{\lambda}_{\mathrm{KS}}/\Delta \ll 1$. Then we can get

$$\dot{\hat{\sigma}}_-^1 = -\frac{\gamma_{\mathrm{Sky}}}{2}\hat{\sigma}_-^1 + i\frac{\bar{\lambda}_{\mathrm{KS}}^2}{\Delta}\hat{\sigma}_-^2\hat{\sigma}_z^1, \tag{97a}$$

$$\dot{\hat{\sigma}}_-^2 = -\frac{\gamma_{\mathrm{Sky}}}{2}\hat{\sigma}_-^2 + i\frac{\bar{\lambda}_{\mathrm{KS}}^2}{\Delta}\hat{\sigma}_-^1\hat{\sigma}_z^2. \tag{97b}$$

After that the effective Hamiltonian containing only skyrmion qubits is

$$\hat{H}_{\mathrm{SKS}}^{\mathrm{eff}} = \Lambda_{\mathrm{IC}}\left(\hat{\sigma}_+^1\hat{\sigma}_-^2 + h.c.\right), \tag{98}$$

where the indirect coupling strength is given by $\Lambda_{\mathrm{IC}} \equiv \bar{\lambda}_{\mathrm{KS}}^2/\Delta$.

C. The magnon-Kerr effect

Since the magnon-mediated skyrmion-skyrmion coupling strength is relatively small, we consider the anisotropy of the YIG sphere resulting in the magnon-Kerr effect. The Kerr term is analyzed in detail in the following. Taking into

account the Zeeman energy, demagnetization energy, and magnetocrystalline anisotropy energy, the Hamiltonian of the YIG sphere with volume V_K is

$$H_K = -\int_{V_K} d\tau \boldsymbol{M}\cdot\boldsymbol{B}_K - \frac{\mu_0}{2}\int_{V_K} d\tau \boldsymbol{M}\cdot(\boldsymbol{H}_{\rm de}+\boldsymbol{H}_{\rm an})\,. \tag{99}$$

$\boldsymbol{B}_K$, $\boldsymbol{H}_{\rm de} = -\boldsymbol{M}/3$, and $\boldsymbol{H}_{\rm an} = (2K_{\rm an}/M_s^2)M_z\hat{\boldsymbol{e}}_z$ represent bias magnetic field, demagnetization energy, and anisotropy energy, respectively. Only the first-order anisotropy constant $K_{\rm an}$ is considered here.

The nanomagnetic sphere can be treated as a macroscopic spin, and the relationship between the magnetization of the YIG sphere and the macroscopic spin can be expressed as $S_z = M_z V_K/\gamma_e$. With the constants ignored, the Hamiltonian can be simplified to

$$H_K = -\gamma_e B_K S_z - \frac{\mu_0\gamma_e^2 K_{\rm an}}{M_s^2 V_K} S_z^2. \tag{100}$$

Macroscopic spin operators can be bosonized by the Holstein-Primakoff transformation [11]

$$\begin{aligned}\hat{S}_+ &= \sqrt{2S_K - \hat{s}_K^\dagger\hat{s}_K}\,\hat{s}_K,\\ \hat{S}_- &= \hat{s}_K^\dagger\sqrt{2S_K - \hat{s}_K^\dagger\hat{s}_K},\\ \hat{S}_+ &= S_K - \hat{s}_K^\dagger\hat{s}_K.\end{aligned} \tag{101}$$

Then the Hamiltonian of the magnon can be denoted as

$$\hat{H}_K = \omega_K\hat{s}_K^\dagger\hat{s}_K - K\hat{s}_K^\dagger\hat{s}_K\hat{s}_K^\dagger\hat{s}_K, \tag{102}$$

where $\omega_K \approx \gamma_e B_K$ and Kerr coefficient is given by $K = \mu_0\gamma_e^2 K_{\rm an}/(M_s^2 V_K)$. As seen in FIG. S7 (b), the Kerr coefficient K is inversely proportional to the YIG sphere volume V_K. The Kerr coefficient is $K/2\pi = 0.89$ Hz when the radius of the YIG sphere is taken to be $R_K = 100$ nm.

D. The two-magnon drive

Based on the previous study, we conclude that the Kerr effect caused by the anisotropy of YIG spheres alone is extremely weak, thus we apply microwave drive to enhance the Kerr effect of YIG spheres. The linearization of the Kerr term to generate the two-magnon drive is analyzed in detail in this section. The Hamiltonian of two skyrmions interacting with the same YIG sphere is

$$\hat{H}_{\rm NSKS} = \frac{\omega_q}{2}(\hat{\sigma}_z^1+\hat{\sigma}_z^2) + \omega_K\hat{s}_K^\dagger\hat{s}_K + \bar{\lambda}_{\rm KS}(\hat{s}_K+\hat{s}_K^\dagger)(\hat{\sigma}_x^1+\hat{\sigma}_x^2) - K\hat{s}_K^\dagger\hat{s}_K\hat{s}_K^\dagger\hat{s}_K + \hat{H}_d, \tag{103}$$

where $\hat{H}_d = \Omega_d(\hat{s}_K^\dagger e^{-i\omega_d t} + \hat{s}_K e^{i\omega_d t})$ with Ω_d representing the drive strength describes the microwave drive. Transforming to a rotating frame with drive frequency ω_d, the Hamiltonian Eq. (103) can be simplified to

$$\hat{H}_{\rm NSKS} = \frac{\Delta_q}{2}\left(\hat{\sigma}_z^1+\hat{\sigma}_z^2\right) + \widetilde{\Delta}_K\hat{s}_K^\dagger\hat{s}_K + \bar{\lambda}_{\rm KS}\left(\hat{s}_K\hat{\sigma}_+^1 + \hat{s}_K\hat{\sigma}_+^2 + h.c.\right) - K\hat{s}_K^\dagger\hat{s}_K\hat{s}_K^\dagger\hat{s}_K + \Omega_d\left(\hat{s}_K+\hat{s}_K^\dagger\right), \tag{104}$$

where $\Delta_q = \omega_q - \omega_d$ and $\Delta_K = \omega_K - K - \omega_d$. Next, utilizing equation $\dot{\hat{A}} = i[\hat{H},\hat{A}]$, the dynamical equation for the magnon can be represented by

$$\dot{\hat{s}}_K = -i\Delta_K\hat{s}_K - i\bar{\lambda}_{\rm KS}\left(\hat{\sigma}_-^1+\hat{\sigma}_+^2\right) + 2iK\hat{s}_K^\dagger\hat{s}_K\hat{s}_K - i\Omega_d. \tag{105}$$

By the strong microwave driving $\hat{H}_d$, we can represent the operator as its expected value plus its associated fluctuation $\hat{A}\to\langle\hat{A}\rangle+\hat{A}$. Omitting the higher-order fluctuation terms in the strong driving condition, the dynamical equation of the magnon can then be simplified to

$$\dot{\hat{s}}_K = -i\Delta_K\hat{s}_K - i\bar{\lambda}_{\rm KS}\left(\hat{\sigma}_-^1+\hat{\sigma}_+^2\right) + 4iK\langle\hat{s}_K\rangle^2\hat{s}_K + 2iK\langle\hat{s}_K\rangle^2\hat{s}_K^\dagger. \tag{106}$$

Then the linearized Hamiltonian can be denoted by

$$\hat{H}_{\rm NSKS} = \frac{\Delta_q}{2}(\hat{\sigma}_z^1+\hat{\sigma}_z^2) + \widetilde{\Delta}_K\hat{s}_K^\dagger\hat{s}_K + \bar{\lambda}_{\rm KS}(\hat{s}_K\hat{\sigma}_+^1+\hat{s}_K\hat{\sigma}_+^2+h.c.) - \frac{K_d}{2}(\hat{s}_K^{\dagger 2}+\hat{s}_K^2), \tag{107}$$

where detuning $\Delta_q = \omega_q - \omega_d$ and $\widetilde{\Delta}_K = \Delta_K - 4K\langle\hat{s}_K\rangle^2$ with $\Delta_K = \omega_K - K - \omega_d$, and enhanced Kerr coefficient is determined by $K_d = 2K\langle\hat{s}_K\rangle^2$.

E. Direct coupling vs. indirect coupling

Based on the preceding analysis, we compare the direct and indirect coupling of qubits in this section. The interaction between two skyrmion qubits can be mediated via the exchange of virtual magnons (long range), with the strength $\Lambda_{\rm IC}=\bar{\lambda}_{\rm KS}^2/\Delta_K$. The direct coupling between skyrmion qubits is described by $\mathcal{H}_{\rm dir}=-J_{\rm dir}\bar{S}^2\int d\boldsymbol{r}\boldsymbol{s}_1\cdot\boldsymbol{s}_2$, where $J_{\rm dir}/2\pi=\mu_0\mu_B^2\bar{S}^2/[\hbar 4\pi^2(2d_{\rm dip})^3]$ is the strength of the interaction between two dipoles in vacuum. Here, $d_{\rm dip}$ denotes the vertical distance of two $\mathfrak{S}_z$ qubits separated by a non-magnetized layer. After quantizing $\mathcal{H}_{\rm dir}$, the direct coupling strength is given by $\Lambda_{\rm DC}=2\pi J_{\rm dir}\bar{S}^2\int\rho d\rho\sin^2\Theta_0$. As illustrated in Fig. S8(a), the long range coupling strength between skyrmion qubits is *three orders of magnitude greater* than the direct one.

To further enhance this magnon-mediated interaction, we take into account the YIG sphere's anisotropic energy, which results in the magnon-Kerr effect. A microwave drive is used to enhance the Kerr effect of the YIG sphere, which is described by $\hat{H}_d=\Omega_d(\hat{s}_K^\dagger e^{-i\omega_d t}+\hat{s}_K e^{i\omega_d t})$, with drive strength Ω_d. Under the strong microwave driving condition, the hybrid system can be described by the Hamiltonian

$$\hat{H}_{\rm NSKS}=\Delta_q/2(\hat{\sigma}_z^1+\hat{\sigma}_z^2)+\widetilde{\Delta}_K\hat{s}_K^\dagger\hat{s}_K+\bar{\lambda}_{\rm KS}(\hat{s}_K\hat{\sigma}_+^1+\hat{s}_K\hat{\sigma}_+^2+{\rm H.c.})-K_d/2(\hat{s}_K^{\dagger 2}+\hat{s}_K^2),\tag{108}$$

where $\Delta_q=\omega_q-\omega_d$, $\widetilde{\Delta}_K=\Delta_K-4K\langle\hat{s}_K\rangle^2$, with $\Delta_K=\omega_K-K-\omega_d$, and the enhanced Kerr coefficient is determined by $K_d=2K\langle\hat{s}_K\rangle^2$. Utilizing the Bogoliubov transformation $\hat{m}=\hat{s}_K\cosh r-\hat{s}_K^\dagger\sinh r$, with $\tanh(2r)=K_d/\widetilde{\Delta}_K$, the Hamiltonian $\hat{H}_{\rm NSKS}$ can be expressed as

$$\hat{H}_{\rm NSKS}^{\rm Sq}=\Delta_q/2(\hat{\sigma}_z^1+\hat{\sigma}_z^2)+\Delta_K^{\rm eff}\hat{m}^\dagger\hat{m}+\lambda_{\rm KS}^{\rm eff}(\hat{m}+\hat{m}^\dagger)(\hat{\sigma}_x^1+\hat{\sigma}_x^2),\tag{109}$$

where $\Delta_K^{\rm eff}=\widetilde{\Delta}_K/\cosh(2r)$ and $\lambda_{\rm KS}^{\rm eff}=\bar{\lambda}_{\rm KS}\exp(r)/2$. *The coupling strength* of the YIG sphere and the skyrmion qubit *is enhanced exponentially*. For simplicity, we assume $\Delta_q=0$. Applying the Schrieffer-Wolff transformation $U=e^{\epsilon\hat{Z}}$ to $\hat{H}_{\rm NSKS}^{\rm Sq}$, with $\epsilon=-i$ and $\hat{Z}=i\lambda_{\rm KS}^{\rm eff}/\Delta_K^{\rm eff}(\hat{m}^\dagger-\hat{m})(\hat{\sigma}_x^1+\hat{\sigma}_x^2)$, the magnon modes can be adiabatically eliminated to obtain the effective skyrmion-skyrmion interaction, i.e.

$$\hat{H}_{\rm NSKS}^{\rm eff}=\Lambda_{\rm KS}^{\rm eff}(\hat{\sigma}_x^1+\hat{\sigma}_x^2)^2.\tag{110}$$

Figure S8(b) illustrates that the magnon-mediated effective skyrmion-skyrmion coupling strength $\Lambda_{\rm KS}^{\rm eff}={\lambda_{\rm KS}^{\rm eff}}^2/\Delta_K^{\rm eff}$ is exponentially enhanced. And it can reach the strong-coupling regime as shown in the shaded area. Performing the dynamical evolution with the Hamiltonian $\hat{H}_{\rm NSKS}^{\rm Sq}$ [Fig. S8(c)], without magnon squeezing ($r=0$), the interaction between the two skyrmions is weak and there is no direct state conversion between the two skyrmions. However, when the parametric drive is added ($r=2$), the skyrmion-skyrmion interaction is exponentially enhanced and the direct state conversion appears. Since the large detuning condition $\Delta_K^{\rm eff}\gg\lambda_{\rm KS}^{\rm eff}$ for the magnon must be satisfied for the Schrieffer-Wolff transformation, the magnon mode is then in virtual excitations and their occupations always approximate zero [Fig. S8(c)]. As shown in Fig. S8(d), the state conversion between two qubits is robust against magnon dissipation.

F. Feasibility analysis of parametric amplification

This section discusses the feasibility of parametric amplification. The relationship between the driving field B_0 and drive power is $B_0=1/R_K\sqrt{2P\mu_0/(\pi c)}$, where P is the driving power, μ_0 the vacuum permeability and c the speed of light. In the following, we calculate the conditions satisfied by the drive power P, and the equation of motion for the magnon annihilation operator is

$$\dot{\hat{s}}_K=-i\left(\Delta_K-i\frac{\gamma_K}{2}\right)\hat{s}_K+iK\hat{s}_K^\dagger\hat{s}_K\hat{s}_K-i\bar{\lambda}_{\rm KS}\hat{\sigma}_--i\Omega_d+M_{\rm in},\tag{111}$$

where $\Delta_K=\omega_K-\omega_d$ is the detuning of the magnon and the microwave drive, γ_K is the decay of the magnon, and $M_{\rm in}$ is the vacuum fluctuation noise satisfying $\langle M_{\rm in}\rangle=0$. The equation of motion for the expectation $\langle\hat{s}_K\rangle$ is then

$$\partial_t\langle\hat{s}_K\rangle=-i\left(\Delta_K-i\frac{\gamma_K}{2}\right)\langle\hat{s}_K\rangle+iK\langle\hat{s}_K^\dagger\hat{s}_K\hat{s}_K\rangle-i\bar{\lambda}_{\rm KS}\langle\hat{\sigma}_-\rangle.\tag{112}$$

Under strong driving conditions, the mean-field approximation results in $\langle\hat{s}_K^\dagger\hat{s}_K\hat{s}_K\rangle=|\langle\hat{s}_K\rangle|^2\langle\hat{s}_K\rangle$. In the long-time limit, $\partial_t\langle\hat{s}_K\rangle=0$, one obtains

$$-i\left(\Delta_K-i\frac{\gamma_K}{2}\right)\langle\hat{s}_K\rangle+iK\langle\hat{s}_K^\dagger\hat{s}_K\hat{s}_K\rangle-i\bar{\lambda}_{\rm KS}\langle\hat{\sigma}_-\rangle=0.\tag{113}$$

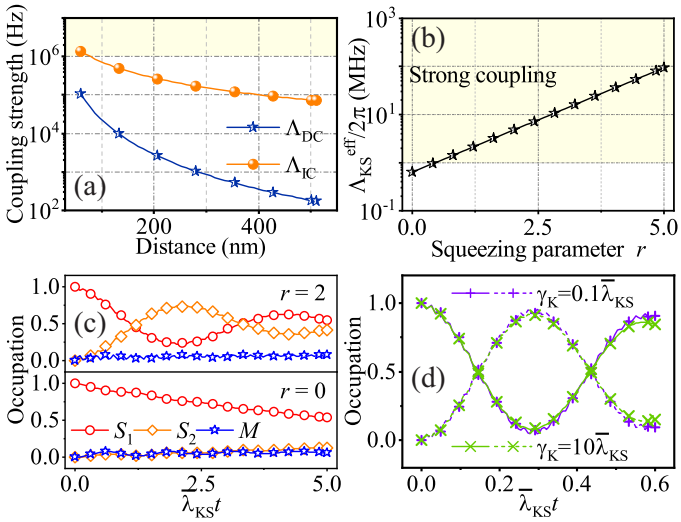

FIG. S8. (a) Comparison of the coupling strength between the direct coupling (dipole-dipole interaction) and indirect coupling (magnon-mediated interaction). (b) The effective skyrmion-skyrmion coupling strength Λ_{KS}^{eff} versus the squeezing parameter r. Logarithmic coordinates are utilized in figures (a, b). (c) Dynamical evolution of the system without ($r = 0$) and with ($r = 2$) magnon squeezing, with $\gamma_K = 0.1\bar{\lambda}_{KS}$. The S_1, S_2, and M correspond to the occupation of the first skyrmion, second skyrmion, and magnon mode, respectively. The robustness of the evolution to the magnon dissipation is presented in (d) with $r = 4$. The solid and dashed curves denote the first skyrmion and second skyrmion, respectively. The other parameters are $\gamma_{Sky} = 0.1\bar{\lambda}_{KS}$ and $\Delta_K^{eff} = 10\lambda_{KS}^{eff}$.

Then we can get

$$\langle \hat{s}_K \rangle = \frac{-\Omega_d}{(\Delta_K - i\frac{\gamma_K}{2}) - K|\langle \hat{s}_K \rangle|^2}, \tag{114}$$

where we have omitted $\bar{\lambda}_{KS}\langle \hat{\sigma}_- \rangle$ due to the small $\bar{\lambda}_{KS}$. The average magnon number can then be defined as

$$N_K = |\langle \hat{s}_K \rangle|^2 = \frac{\Omega_d^2}{(\Delta_K - K|\langle \hat{s}_K \rangle|^2)^2 + \gamma_K^2/4}. \tag{115}$$

We can assume that $\langle \hat{s}_K \rangle$ is a real number by adjusting the phase of the microwave driving field. Consequently,

$$\Omega_d = \sqrt{N_K\left[(\Delta_K - KN_K)^2 + \gamma_K^2/4\right]} \tag{116}$$

is obtained. According to Eq. (116), $B_0 = 1/R_K\sqrt{2P\mu_0/(\pi c)}$, $\Omega_d = \sqrt{5}/4\gamma_e\sqrt{N}B_0$, and the definition of the squeezing parameter $r = 1/4\ln[(\widetilde{\Delta}_K + K_d)/(\widetilde{\Delta}_K - K_d)]$, we can obtain the relationship between the squeezing parameter r and the drive power P, where $\widetilde{\Delta}_K = \Delta_K - 4KN_K$, $K_d = 2KN_K$, and N is the number of spins in the YIG sphere. When the detuning Δ_K is given, as illustrated in Fig. S9(a), the correspondence between the driving power P and the squeezing parameter r is given.

Next,, we examine the limits of drive power. It must satisfy the requirement $\widetilde{\Delta}_K > K_d$ according to the definition of the squeezing parameter $r = 1/4\ln[(\widetilde{\Delta}_K + K_d)/(\widetilde{\Delta}_K - K_d)]$. Then,

$$|\langle \hat{s}_K \rangle|^2 = \frac{\Omega_d^2}{(\Delta_K - K|\langle \hat{s}_K \rangle|^2)^2 + \gamma_K^2/4} < \frac{\Delta_K}{6K} \Rightarrow 6\Omega_d^2 K < \Delta_K\left[\left(\Delta_K - K|\langle \hat{s}_K \rangle|^2\right)^2 + \frac{\gamma_K^2}{4}\right] \equiv f(\Delta_K) \tag{117}$$

can be obtained. It is only necessary to fulfill

$$6\Omega_d^2 K < f_{\min}(\Delta_K) = \frac{\Delta_K \gamma_K^2}{4} \Rightarrow \Omega_d < \frac{\gamma_K}{2}\sqrt{\frac{\Delta_K}{6K}} \tag{118}$$

to meet the preceding conditions. With $\Omega_d = \gamma_e\sqrt{10NP\mu_0}/(4R\sqrt{\pi c})$, we can determine an upper bound for the driving power. $N_K^{\max}$ is the average number of magnon excitations N_K that correspond to the top drive power limit. In addition to this upper limit, the number of magnon excitations must meet the requirements of $N_K \ll 2Ns \equiv N_{\text{tot}}$, i.e., be low-excitation. Figure S9(b) depicts the variation of $N_K^{\max}$ with detuning Δ_K. The magnon's average excitation number should fall inside the low excitation area shown in Fig. S9(b).

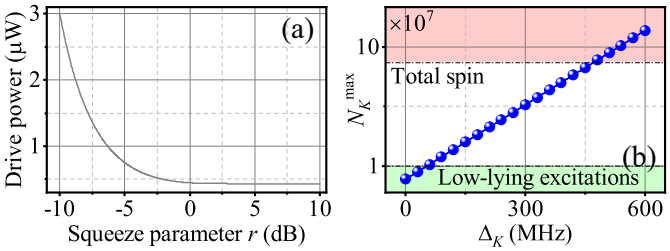

FIG. S9. (a) Relationship between driving power P and squeezing parameter r. (b) $N_K^{\max}$ as a function of detuning Δ_K. The parameters used are $R_K = 100$ nm, the spin density $\rho_s = 4.22 \times 10^{27}$ m^{-3}, the spin number of the ground-state Fe^{3+} ion in YIG $s = 5/2$, $N = \rho_s V_K$, $N_K = |\langle \hat{s}_K \rangle|^2 = 10^7$, and the total spin $N_{\rm tot} = 2Ns = 8.8 \times 10^7$.

V. NONRECIPROCAL INTERACTIONS BETWEEN SKYRMION QUBITS

A. Microwave drive to skyrmion qubits

The microwave-driven Hamiltonian is computed in the same method as the interaction Hamiltonian as illustrated in Sec. III. With the microwave drive $\boldsymbol{B}_{\rm mw} = B_0 \cos(\omega_{\rm mw} t)\, \hat{\boldsymbol{e}}_z$ polarized in the z direction, the Hamiltonian of the microwave drive can be expressed as

$$\hat{H}_{\rm mw} = \Omega_{\rm mw} \cos(\omega_{\rm mw} t)\, \hat{\sigma}_z^{\rm sub} \tag{119}$$

where B_0 is the amplitude of the microwave drive and $\omega_{\rm mw}$ is the frequency of the microwave drive. The strength of the microwave drive is defined as $\Omega_{\rm mw} \equiv g\mu_B B_0 \bar{S}/2$. It should be noted that Eq. (119) is expanded under the subspace $\{|0\rangle, |1\rangle\}$. Transforming to the diagonal basis $\{|\psi_+\rangle, |\psi_-\rangle\}$ of the skyrmion qubits, the microwave-driven Hamiltonian can be reduced to

$$\hat{H}_{\rm mw} = \Omega_{\rm mw} \cos(\omega_{\rm mw} t)\, \hat{\sigma}_x \tag{120}$$

where $\cos(2\theta) \sim 0$ and $\sin(2\theta) \sim 1$ have been used.

B. The effective Rabi coupling

In the previous part, we discussed coherent coupling between qubits mediated by magnons, which was exponentially enhanced with a two-magnon drive. In this part, we employ magnon dissipation to mediate an non-reciprocal dissipative coupling between skyrmion qubits, and the prior section's strategy of two-magnon drive to increase coupling strength also works here. The hybrid system's Hamiltonian is given by

$$\hat{H}_{\rm SKSD} = \frac{\omega_q}{2}(\hat{\sigma}_z^1 + \hat{\sigma}_z^2) + \omega_K \hat{s}_K^\dagger \hat{s}_K + \bar{\lambda}_{\rm KS}\left(\hat{s}_K \hat{\sigma}_+^1 + \hat{s}_K^\dagger \hat{\sigma}_-^1\right) + \bar{\lambda}_{\rm KS}\left(\hat{s}_K \hat{\sigma}_+^2 + \hat{s}_K^\dagger \hat{\sigma}_-^2\right) + \hat{H}_d, \tag{121}$$

where two qubits are coupled to the same YIG sphere, one of which is driven by microwaves with $\hat{H}_{\rm qd} = -\Omega_1(e^{i\omega_1 t}\hat{\sigma}_-^1 + e^{-i\omega_1 t}\hat{\sigma}_+^1) - \Omega_2(e^{i\omega_2 t}\hat{\sigma}_-^1 + e^{-i\omega_2 t}\hat{\sigma}_+^1)$, where $\Omega_{1/2}$ and $\omega_{1/2}$ are the driving strength and frequency, respectively. Transforming to the rotating frame of drive Ω_1 yields

$$\begin{aligned} \hat{H}_{\rm SKSD} = &\frac{\Delta_{q,1}}{2}\hat{\sigma}_z^1 + \frac{\Delta_{q,1}}{2}\hat{\sigma}_z^2 + \Delta_{K,1}\hat{s}_K^\dagger \hat{s}_K + \bar{\lambda}_{\rm KS}\left(\hat{s}_K \hat{\sigma}_+^1 + \hat{s}_K^\dagger \hat{\sigma}_-^1\right) + \bar{\lambda}_{\rm KS}\left(\hat{s}_K \hat{\sigma}_+^2 + \hat{s}_K^\dagger \hat{\sigma}_-^2\right), \\ &- \Omega_1\left(\hat{\sigma}_-^1 + \hat{\sigma}_+^1\right) - \Omega_2\left[e^{i(\omega_2-\omega_1)t}\hat{\sigma}_-^1 + e^{-i(\omega_2-\omega_1)t}\hat{\sigma}_+^1\right], \end{aligned} \tag{122}$$

where $\Delta_{q,1} = \omega_q - \omega_1$ and $\Delta_{K,1} = \omega_K - \omega_1$. After the transformation described above, we convert the first drive into a time-independent term and assume that it is the most significant term, defined as $\hat{H}_0 = -\Omega_1(\hat{\sigma}_-^1 + \hat{\sigma}_+^1)$. Employing the transformation $\hat{H}_{\rm SKSJR} = \exp(i\hat{H}_0 t)(\hat{H}_{\rm SKSD} - \hat{H}_0)\exp(-i\hat{H}_0 t)$ and the rotational spin basis $|\pm\rangle = (|\psi_-\rangle \pm |\psi_+\rangle)/\sqrt{2}$,

one obtains

$$\begin{aligned}\hat{H}_{\mathrm{SKSJR}} &= \frac{\Delta_{q,1}}{2}\left(e^{-i2\Omega_1 t}|+\rangle\langle -|+h.c.\right)+\frac{\Delta_{q,1}}{2}\hat{\sigma}_z^2+\Delta_{K,1}\hat{s}_K^\dagger\hat{s}_K\\&+\frac{\bar{\lambda}_{\mathrm{KS}}}{2}\left[\left(|+\rangle\langle +|-|-\rangle\langle -|+e^{-i2\Omega_1 t}|+\rangle\langle -|-e^{-i2\Omega_1 t}|-\rangle\langle +|\right)\hat{s}_K+h.c.\right]\\&-\frac{\Omega_2}{2}\left[\left(|+\rangle\langle +|-|-\rangle\langle -|-e^{-i2\Omega_1 t}|+\rangle\langle -|+e^{i2\Omega_1 t}|-\rangle\langle +|\right)e^{i(\omega_2-\omega_1)t}+h.c.\right]\\&+\bar{\lambda}_{\mathrm{KS}}\left(\hat{s}_K\hat{\sigma}_+^2+\hat{s}_K^\dagger\hat{\sigma}_-^2\right).\end{aligned}\tag{123}$$

By adjusting the drive frequency to satisfy $\omega_1-\omega_2=2\Omega_1$ and assuming that drive Ω_1 is sufficiently strong, the Hamiltonian (123) can be reduced to

$$\hat{H}_{\mathrm{SKSD}}=\frac{\Omega_2}{2}\hat{\sigma}_z^1+\frac{\Delta_{q,1}}{2}\hat{\sigma_z}^2+\Delta_{K,1}\hat{s}_K^\dagger\hat{s}_K+\frac{\bar{\lambda}_{\mathrm{KS}}}{2}\left(\hat{s}_K+\hat{s}_K^\dagger\right)\hat{\sigma}_x^1+\bar{\lambda}_{\mathrm{KS}}\left(\hat{s}_K\hat{\sigma}_+^2+\hat{s}_K^\dagger\hat{\sigma}_-^2\right).\tag{124}$$

In other words, in a single system, we possess both JC coupling and effective Rabi coupling.

C. The nonreciprocal interaction

When the magnon dissipation is large, we can achieve dissipative coupling between skyrmion qubits by adiabatically eliminating the magnon modes. The system's Lindblad master equation is given by

$$\dot{\hat{\rho}}=-i\left[\hat{H}_{\mathrm{SKSD}},\hat{\rho}\right]+\gamma_K D[\hat{s}_K]\hat{\rho},\tag{125}$$

where $D[\hat{O}]\hat{\rho}=\hat{O}\hat{\rho}\hat{O}^\dagger-\{\hat{O}^\dagger\hat{O},\hat{\rho}\}/2$ is the Lindblad operator and γ_K is the magnon dissipation. The equation of motion for the annihilation operator $\hat{s}_K$ is given by

$$\dot{\hat{s}}_K=-i\Delta_{K,1}\hat{s}_K-ig\left(\frac{1}{2}\hat{\sigma}_+^1+\frac{1}{2}\hat{\sigma}_-^1+\hat{\sigma}_-^2\right)-\frac{\gamma_K}{2}\hat{s}_K.\tag{126}$$

In the bad-cavity limit $\gamma_K\gg\bar{\lambda}_{\mathrm{KS}}$, the magnon mode can be eliminated adiabatically, i.e., $\dot{\hat{s}}_K=0$, yielding

$$\hat{s}_K=\frac{-i\bar{\lambda}_{\mathrm{KS}}\left(\frac{1}{2}\hat{\sigma}_+^1+\frac{1}{2}\hat{\sigma}_-^1+\hat{\sigma}_-^2\right)}{i\Delta_{K,1}+\gamma_K/2},\ \hat{s}_K^\dagger=\frac{i\bar{\lambda}_{\mathrm{KS}}\left(\frac{1}{2}\hat{\sigma}_-^1+\frac{1}{2}\hat{\sigma}_+^1+\hat{\sigma}_+^2\right)}{-i\Delta_{K,1}+\gamma_K/2}.\tag{127}$$

After calculating, we can get

$$\begin{aligned}\hat{s}_K\hat{\sigma}_-^1&=\frac{-i\bar{\lambda}_{\mathrm{KS}}\left(\frac{1}{2}\hat{\sigma}_+^1\hat{\sigma}_-^1+\frac{1}{2}\hat{\sigma}_-^1\hat{\sigma}_-^1+\hat{\sigma}_-^2\hat{\sigma}_-^1\right)}{\Delta_{K,1}^2+\gamma_K^2/4},\ \hat{\sigma}_+^1\hat{s}_K^\dagger=\frac{i\bar{\lambda}_{\mathrm{KS}}\left(\frac{1}{2}\hat{\sigma}_+^1\hat{\sigma}_-^1+\frac{1}{2}\hat{\sigma}_+^1\hat{\sigma}_+^1+\hat{\sigma}_+^1\hat{\sigma}_+^2\right)}{\Delta_{K,1}^2+\gamma_K^2/4},\\\hat{s}_K\hat{\sigma}_+^1&=\frac{-i\bar{\lambda}_{\mathrm{KS}}\left(\frac{1}{2}\hat{\sigma}_+^1\hat{\sigma}_+^1+\frac{1}{2}\hat{\sigma}_-^1\hat{\sigma}_+^1+\hat{\sigma}_-^2\hat{\sigma}_+^1\right)}{\Delta_{K,1}^2+\gamma_K^2/4},\ \hat{\sigma}_-^1\hat{s}_K^\dagger=\frac{i\bar{\lambda}_{\mathrm{KS}}\left(\frac{1}{2}\hat{\sigma}_-^1\hat{\sigma}_-^1+\frac{1}{2}\hat{\sigma}_-^1\hat{\sigma}_+^1+\hat{\sigma}_-^1\hat{\sigma}_+^2\right)}{\Delta_{K,1}^2+\gamma_K^2/4},\\\hat{s}_K\hat{\sigma}_+^2&=\frac{-i\bar{\lambda}_{\mathrm{KS}}\left(\frac{1}{2}\hat{\sigma}_+^1\hat{\sigma}_+^2+\frac{1}{2}\hat{\sigma}_-^1\hat{\sigma}_+^2+\hat{\sigma}_-^2\hat{\sigma}_+^2\right)}{\Delta_{K,1}^2+\gamma_K^2/4},\ \hat{\sigma}_-^2\hat{s}_K^\dagger=\frac{i\bar{\lambda}_{\mathrm{KS}}\left(\frac{1}{2}\hat{\sigma}_-^2\hat{\sigma}_-^1+\frac{1}{2}\hat{\sigma}_-^2\hat{\sigma}_+^1+\hat{\sigma}_-^2\hat{\sigma}_+^2\right)}{\Delta_{K,1}^2+\gamma_K^2/4},\\\hat{s}_K^\dagger\hat{s}_K&=\frac{\bar{\lambda}_{\mathrm{KS}}^2\left(\frac{1}{4}\hat{\sigma}_-^1\hat{\sigma}_+^1+\frac{1}{4}\hat{\sigma}_-^1\hat{\sigma}_-^1+\frac{1}{2}\hat{\sigma}_-^1\hat{\sigma}_-^2\right)}{\Delta_{K,1}^2+\gamma_K^2/4}+\frac{\bar{\lambda}_{\mathrm{KS}}^2\left(\frac{1}{4}\hat{\sigma}_+^1\hat{\sigma}_+^1+\frac{1}{4}\hat{\sigma}_+^1\hat{\sigma}_-^1+\frac{1}{2}\hat{\sigma}_+^1\hat{\sigma}_-^2\right)}{\Delta_{K,1}^2+\gamma_K^2/4}\\&+\frac{\bar{\lambda}_{\mathrm{KS}}^2\left(\frac{1}{2}\hat{\sigma}_+^2\hat{\sigma}_+^1+\frac{1}{2}\hat{\sigma}_+^2\hat{\sigma}_-^1+\hat{\sigma}_+^2\hat{\sigma}_-^2\right)}{\Delta_{K,1}^2+\gamma_K^2/4}.\end{aligned}\tag{128}$$

Substituting Eq. (128) into the master equation (125) yields the master equations

$$\dot{\hat{\rho}}=-i[\hat{H}_{\mathrm{coh}},\hat{\rho}]+\Gamma D[\hat{\Sigma}_-]\hat{\rho}\tag{129}$$

and

$$\hat{H}_{\mathrm{coh}}=\frac{1}{2}\mathcal{W}_1\hat{\sigma}_z^1+\frac{1}{2}\mathcal{W}_2\hat{\sigma}_z^2-\mathcal{G}\hat{\sigma}_x^1\hat{\sigma}_x^2,\tag{130}$$

where Eq. (130) represents the magnon-mediated coherent coupling between the qubits and $D[\hat{\Sigma}_-]\hat{\rho}$ represents the magnon-mediated dissipative coupling between the qubits with $\hat{\Sigma}_- \equiv 1/2\hat{\sigma}_+^1 + 1/2\hat{\sigma}_-^1 + \hat{\sigma}_-^2$. The parameters in master equation (129) and Hamiltonian (130) are defined as

$$\mathcal{W}_1 = \Omega_2,\ \mathcal{W}_2 = \Delta_{q,1} - \frac{\Delta_{K,1}\bar{\lambda}_{\mathrm{KS}}^2}{\Delta_{K,1}^2 + \gamma_K^2/4},\ \mathcal{G} = \frac{1}{2}\frac{\Delta_{K,1}\bar{\lambda}_{\mathrm{KS}}^2}{\Delta_{K,1}^2 + \gamma_K^2/4},\ \Gamma = \frac{\gamma_K\bar{\lambda}_{\mathrm{KS}}^2}{\Delta_{K,1}^2 + \gamma_K^2/4}. \tag{131}$$

The quantum Langevin equations (QLEs) of the system can be represented as

$$\begin{aligned}
\dot{\hat{\sigma}}_-^1 &= (-i\mathcal{W}_1 - \frac{\Gamma}{4})\hat{\sigma}_-^1 + \frac{\Gamma}{4}\hat{\sigma}_+^1 - \left[\left(i\mathcal{G} - \frac{\Gamma}{4}\right)\hat{\sigma}_-^2 + \left(i\mathcal{G} + \frac{\Gamma}{4}\right)\hat{\sigma}_+^2\right]\hat{\sigma}_z^1, \\
\dot{\hat{\sigma}}_-^2 &= (-i\mathcal{W}_2 - \frac{\Gamma}{2})\hat{\sigma}_-^2 - \left[\left(i\mathcal{G} - \frac{\Gamma}{4}\right)\hat{\sigma}_-^1 + \left(i\mathcal{G} - \frac{\Gamma}{4}\right)\hat{\sigma}_+^1\right]\hat{\sigma}_z^2.
\end{aligned} \tag{132}$$

using Eq. (129).The nonlocal damping in Eq. (129) couples the raising and lowering operators of the two qubits; in other words, the nonlocal damping induced by the engineered reservoir mediates a nonlocal damping force on each qubit. Furthermore, the dissipative coupling is asymmetric, allowing for nonreciprocal population conversion. With the value $\mathcal{W}_1 = \mathcal{W}_2 = \mathcal{G} = 0$, the simplified QELs in the main text are obtained.

VI. THE SKYRMION-MAGNON-NV HYBRID SYSTEM

A. The magnon-NV interaction

This section illustrates the analysis of the magnon-NV interaction. For the convenience of calculation, we establish a local coordinate system $x'y'z'$ with the center of the YIG sphere as the origin and the magnetization direction as the positive direction of z' axis. The NV center is placed directly above the magnetic sphere, at a distance h_{NV} from the center of the sphere [FIG. S10(a)]. Then the position vector of the magnetic sphere to the NV center is $\boldsymbol{r}_{\mathrm{KN}} = (h_{\mathrm{NV}}, 0, 0)$. In the local coordinate, the quantized magnetization operator is given by $\hat{\boldsymbol{M}} = [\widetilde{\boldsymbol{m}}_K\hat{s}_K + \widetilde{\boldsymbol{m}}_K^*\hat{s}_K^\dagger]$ with the Kittel mode function $\widetilde{\boldsymbol{m}}_K = \hat{\boldsymbol{e}}_{x'} + i\hat{\boldsymbol{e}}_{y'}$. Then we can derive the quantized magnetic field

$$\hat{B}_{x'} = \frac{\mu_0 V_K}{4\pi}\frac{2M_K\left(\hat{s}_K + \hat{s}_K^\dagger\right)}{h_{\mathrm{NV}}^3}, \tag{133a}$$

$$\hat{B}_{y'} = -\frac{\mu_0 V_K}{4\pi}\frac{iM_K\left(\hat{s}_K - \hat{s}_K^\dagger\right)}{h_{\mathrm{NV}}^3}. \tag{133b}$$

The interaction between the magnetic sphere and the NV center is described by

$$\hat{H}_{\mathrm{KN}} = -\gamma_e\hat{\boldsymbol{B}}\cdot\hat{\boldsymbol{S}} = -\gamma_e\hat{B}_{x'}\hat{S}_x - \gamma_e\hat{B}_{y'}\hat{S}_y. \tag{134}$$

Exploiting $\hat{S}_x = (\hat{S}_+ + \hat{S}_-)/2$ and $\hat{S}_y = (\hat{S}_+ - \hat{S}_-)/(2i)$, the interaction Hamiltonian is given by

$$\hat{H}_{\mathrm{KN}} = -\lambda_{\mathrm{KN}}\left(\hat{s}_K\hat{S}_+ + \hat{s}_K^\dagger\hat{S}_-\right), \tag{135}$$

where the coupling strength is given by $\lambda_{\mathrm{KN}} = \gamma_e\mu_0 M_K R_K^3/(2h_{\mathrm{NV}}^3)$ [FIG. S10(b)]. Here we have used the rotating wave approximation to neglect the anti-rotation terms $\hat{s}_K^\dagger\hat{S}_+$ and $\hat{s}_K\hat{S}_-$. In the subsequent calculation, we take the radius of the magnetic sphere and the distance from the magnetic sphere to the NV center as $R_K = 100$ nm and $d_{\mathrm{NV}} = 10$ nm, respectively, which results in the magnon-NV coupling strength is $\lambda_{\mathrm{KN}}/2\pi = 0.48$ MHz.

B. The skyrmion-magnon-NV hybrid system

In this section, we will derive the Hamiltonian for the skyrmion-magnon-NV hybrid quantum system in detail. The NV center is situated close to the YIG magnetic sphere, as shown in FIG. S10(a). For a single NV center, the

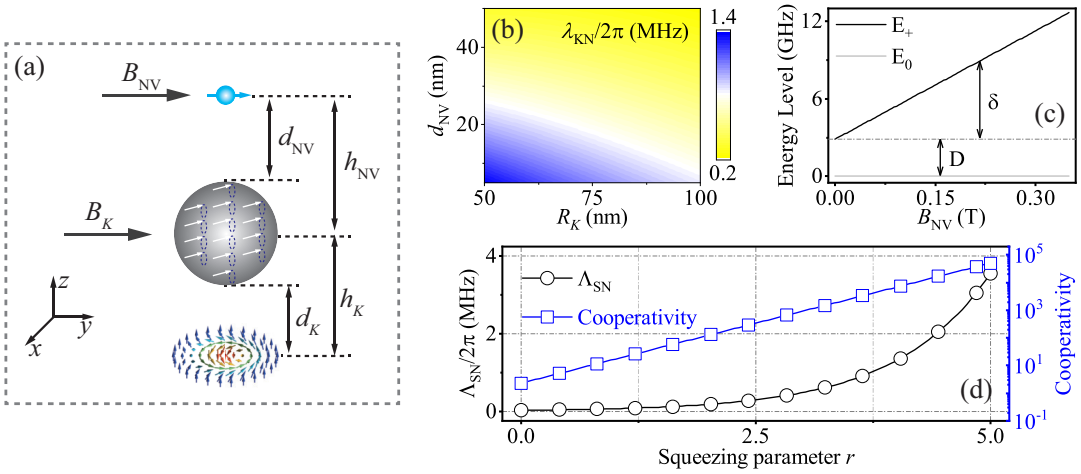

FIG. S10. (a) The skyrmion-magnon-NV hybrid quantum system. Here we take $R_K = 100$ nm and $d_{\rm NV} = 10$ nm. (b) The coupling strength $\lambda_{\rm KN}$ between the NV center and the YIG sphere is plotted as a function of the magnetic sphere's radius R_K and the distance $d_{\rm NV}$ from the magnetic sphere's surface to the NV center. (c) The relationship between the energy level of the spin qubit and the bias magnetic field $B_{\rm NV}$ is illustrated. (d) The magnon-mediated skyrmion-NV interaction strength and cooperativity are displayed as a function of the squeezing parameter r. We apply logarithmic coordinates to the cooperativity. The parameters are $\bar{\lambda}_{\rm KS}/2\pi = 6.35$ MHz, $\lambda_{\rm KN}/2\pi = 0.48$ MHz, $\mathcal{W}_K = 10\lambda_{\rm KS}^{\rm eff}$, $\gamma_{\rm Sky}/2\pi = 1$ MHz, and $\gamma_{\rm NV}/2\pi = 1$ kHz.

ground-state energy level structure is the ground triplet state $|0,\pm1\rangle$, and the zero-field splitting between $|0\rangle$ and degenerate sublevels $|\pm1\rangle$ is $D/2\pi = 2.87$ GHz. When a homogeneous static magnetic field along the z' direction is introduced, the degenerate states $|\pm1\rangle$ can be removed because of the Zeeman effect. Then the NV center is described by

$$\hat{H}_{\rm NV} = D\hat{S}_z^2 + \delta\hat{S}_z, \tag{136}$$

where $\delta = \gamma_e B_{\rm NV}$. FIG. S10(c) shows the tuning of the spin qubit resonance frequency by an applied magnetic field $B_{\rm NV}$. In the subspace $\{|0\rangle, |\pm1\rangle\}$, $\hat{H}_{\rm NV}$ can be reduced to $\hat{H}_{\rm NV} = (D+\delta)|+1\rangle\langle+1| + (D-\delta)|-1\rangle\langle-1|$. Here $|0\rangle$ and $|+1\rangle$ are considered as spin qubits. Then the interaction between the YIG sphere and the NV center is described by

$$\hat{H}_{\rm KN} = -\lambda_{\rm KN}\left(\hat{s}_K\hat{\sigma}_+^{\rm NV} + h.c.\right) \tag{137}$$

with the coupling strength $\lambda_{\rm KN} = \gamma_e\mu_0 M_K R_K^3/(2h_{\rm NV}^3)$. FIG. S10(b) shows the dependence of the spin-magnon coupling strength on the YIG sphere radius R_K and the distance $d_{\rm NV}$ between the YIG sphere surface and the NV center.

The skyrmion-magnon-NV hybrid quantum system can be described by the Hamiltonian

$$\hat{H}_{\rm SKN} = \frac{\Delta_q}{2}\hat{\sigma}_z + \frac{\Delta_{\rm NV}}{2}\hat{\sigma}_z^{\rm NV} + \widetilde{\Delta}_K\hat{s}_K^\dagger\hat{s}_K + \bar{\lambda}_{\rm KS}(\hat{s}_K\hat{\sigma}_+ + h.c.) - \lambda_{\rm KN}(\hat{s}_K\hat{\sigma}_+^{\rm NV} + h.c.) - \frac{K_d}{2}(\hat{s}_K^{\dagger 2} + \hat{s}_K^2) \tag{138}$$

with $\Delta_{\rm NV} = \omega_{\rm NV} - \omega_d$ and $\omega_{\rm NV} = E_+ - E_0$. The Pauli operators for the NV center are defined as $\hat{\sigma}_z^{\rm NV} \equiv |+1\rangle\langle+1| - |0\rangle\langle0|$ and $\hat{\sigma}_+^{\rm NV} \equiv |+1\rangle\langle0|$. Utilizing the Bogoliubov transformation and the rotating-wave approximation (RWA), we can obtain

$$\hat{H}_{\rm SKN}^{\rm Sq} = \frac{\Delta_q}{2}\hat{\sigma}_z + \frac{\Delta_{\rm NV}}{2}\hat{\sigma}_z^{\rm NV} + \Delta_K^{\rm eff}\hat{m}^\dagger\hat{m} + \lambda_{\rm KS}^{\rm eff}(\hat{m}\hat{\sigma}_+ + h.c.) - \lambda_{\rm KN}^{\rm eff}(\hat{m}\hat{\sigma}_+^{\rm NV} + h.c.), \tag{139}$$

where $\Delta_K^{\rm eff} = \widetilde{\Delta}_K/\cosh(2r)$, $\lambda_{\rm KS}^{\rm eff} = \bar{\lambda}_{\rm KS}e^r/2$, $\lambda_{\rm KN}^{\rm eff} = \lambda_{\rm KN}e^r/2$, and $\tanh(2r) = K_d/\widetilde{\Delta}_K$. The coupling strength $\lambda_{\rm KN}^{\rm eff} = \lambda_{\rm KN}\exp(r)/2$ is *enhanced exponentially*. With the large detuning condition, the magnon modes can be adiabatically eliminated to yield the effective skyrmion-NV interaction

$$\hat{H}_{\rm SKN}^{\rm eff} = \Delta_q/2\hat{\sigma}_z + \Delta_{\rm NV}/2\hat{\sigma}_z^{\rm NV} + \Lambda_{\rm SN}(\hat{\sigma}_+\hat{\sigma}_-^{\rm NV} + {\rm H.c.}). \tag{140}$$

$\Lambda_{\rm SN} = \lambda_{\rm KN}^{\rm eff}\lambda_{\rm KS}^{\rm eff}/\mathcal{W}_K$ is the effective coupling strength with $\mathcal{W}_K = \Delta_K^{\rm eff} - \Delta_q$. As shown in Fig. S10(d), the effective coupling strength and cooperativity $\mathcal{C}_{\rm SN} = 4\Lambda_{\rm SN}^2/(\gamma_{\rm NV}\gamma_{\rm Sky})$ are drawn versus the squeezing parameter r. The effective

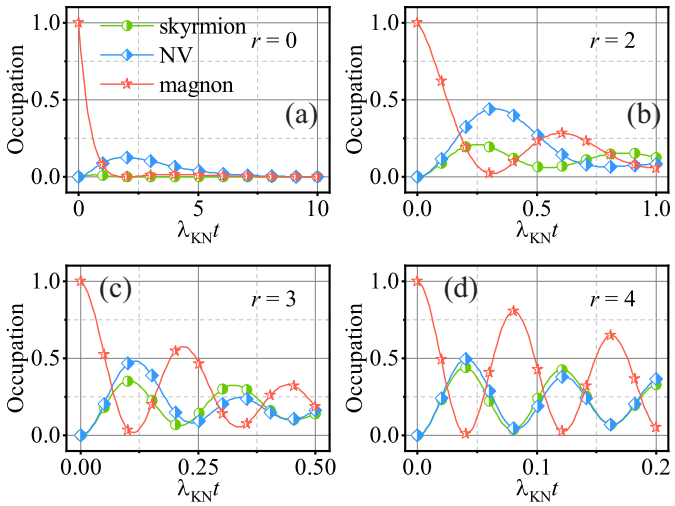

FIG. S11. In the interaction picture, the Hamiltonian Eq. (139) is used to show the dynamical evolution of the skyrmion-magnon-NV hybrid quantum system with different squeezing parameters r. The parameters are $\bar{\lambda}_{\rm KS} = \lambda_{\rm KN}$, and $\gamma_{\rm Sky} = \gamma_K = 2\lambda_{\rm KN}$.

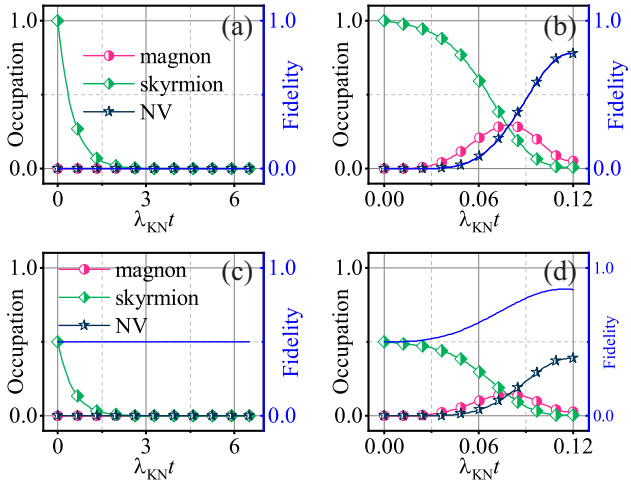

FIG. S12. The dynamical evolution of Fock state conversion without ($r = 0$) and with ($r = 4$) parametric amplification is shown in (a) and (b), respectively, with initial state $|\psi_{\rm Sky}\rangle|\psi_{\rm Mag}\rangle|\psi_{\rm NV}\rangle = |1\rangle|0\rangle|0\rangle$. (c) and (d) show the state conversion of the superposition state without ($r = 0$) and with ($r = 4$) parametric drive, respectively. The parameters of (a) and (c) are $\lambda^{\rm eff}_{\rm KS}(t) = 13(\lambda_{\rm KN}e^r/2)\sin(\pi t/160)$, $\lambda^{\rm eff}_{\rm KN}(t) = (\lambda_{\rm KN}e^r/2)\cos(\pi t/80)$, and $r = 0$, and that in (b) and (d) are $\lambda^{\rm eff}_{\rm KS}(t) = 13(\lambda_{\rm KN}e^r/2)\sin(\pi t/3)$, $\lambda^{\rm eff}_{\rm KN}(t) = (\lambda_{\rm KN}e^r/2)\cos(\pi t)$, and $r = 4$. The other parameters are $\gamma_{\rm Sky} = \gamma_K = 2\lambda_{\rm KN}$.

coupling strength can reach 2.16 MHz when the squeezing parameter r is set to 4.5, where the cooperativity $\mathcal{C}_{\rm SN} \approx 7300 \gg 1$. That is, strong coupling between the skyrmion and the NV center can be mediated by the magnon.

As shown in FIG. S11, the dynamics simulation employing Eq. (139) shows that, in the absence of a parametric drive, there is no energy exchange between the three subsystems due to the weak coupling between the NV center and the YIG sphere. As the parametric drive is introduced and increased, the energy exchange between the three subsystems appears and accelerates.

Through the foregoing analysis, the interaction between the NV center and skyrmion has been mediated. And then, we implement coherent quantum state conversion via the dark state, which is less impacted by the magnon dissipation than direct state conversion [12–16]. We take the resonance condition $\Delta_q \approx \Delta_{\rm NV} \approx \Delta^{\rm eff}_K$ and introduce two polariton operators $\hat{\mathcal{U}}_{\rm br} \equiv \sin\alpha\hat{\sigma}_- + \cos\alpha\hat{\sigma}^{\rm NV}_-$ and $\hat{\mathcal{U}}_{\rm dk} \equiv -\cos\alpha\hat{\sigma}_- + \sin\alpha\hat{\sigma}^{\rm NV}_-$ with $\tan\alpha = -\lambda^{\rm eff}_{\rm KS}/\lambda^{\rm eff}_{\rm KN}$. Defining the hybrid modes $\hat{\mathcal{U}}_\pm \equiv (\hat{U}_{\rm br} \pm \hat{m})/\sqrt{2}$, the hybrid system's Hamiltonian can be diagonalized $\hat{H}^{\rm diag}_{\rm SKN} = \omega_{\rm dk}\hat{\mathcal{U}}^\dagger_{\rm dk}\hat{\mathcal{U}}_{\rm dk} + \omega_+\hat{\mathcal{U}}^\dagger_+\hat{\mathcal{U}}_+ + \omega_-\hat{\mathcal{U}}^\dagger_-\hat{\mathcal{U}}_-$ with $\omega_\pm = \omega_{\rm dk} \pm \sqrt{{\lambda^{\rm eff}_{\rm KS}}^2 + {\lambda^{\rm eff}_{\rm KN}}^2}$ and $\omega_{\rm dk} = \Delta^{\rm eff}_K$, implying three mutually independent excitations. We

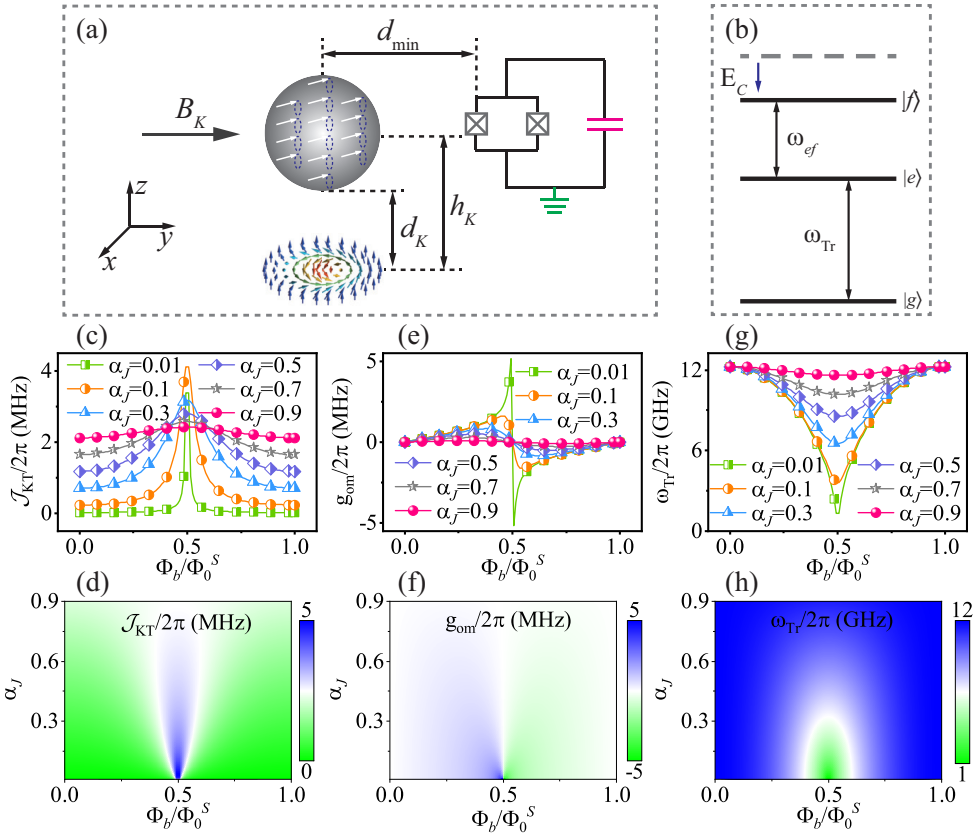

FIG. S13. (a) The model of the skyrmion-magnon-SQ hybrid quantum system. (b) Energy levels of transmon qubit. The variations of $\mathcal{J}_{\rm KT}$, $g_{\rm om}$, and $\omega_{\rm Tr}$ with parameter Φ_b/Φ_0^S for a given α_J are shown in (c), (e), and (g), respectively. $\mathcal{J}_{\rm KT}$, $g_{\rm om}$, and $\omega_{\rm Tr}$ are depicted as functions of Φ_b/Φ_0^S and α_J in (d), (f), and (h), respectively.

are interested in the polaron $\hat{\mathcal{U}}_{\rm dk}$ because it misses the magnon mode, which indicates that the magnon mode is in a dark state. We find that $\hat{\mathcal{U}}_{\rm dk} = -\hat{\sigma}_-$ when $\alpha = 0$, and $\hat{\mathcal{U}}_{\rm dk} = \hat{\sigma}_-^{\rm NV}$ when $\alpha = \pi/2$. As we evolve α adiabatically from 0 to $\pi/2$, we can enable the quantum state conversion from the skyrmion qubit to the NV center. As illustrated in FIG. S12, We employ the Hamiltonian $\hat{H}_{\rm SKN}^{\rm Sq}$ for the dynamical evolution in the interaction picture. Without a parametric drive [FIG. S12(a)], even employing the dark state conversion technique, the quantum state conversion between the two subsystems is impossible because the coupling strength of the NV center and YIG sphere is weak. When the parametric drive is introduced [FIG. S12(b)], the system's coupling strength is enhanced exponentially, enabling the realization of quantum state conversion and dramatically accelerating the speed of state conversion. Except for the transfer of Fock states, the skyrmion-magnon-NV hybrid quantum system can also realize the state transfer of superposition states, as shown in FIG. S12(c) and (d). The initial states of the skyrmion, magnon, and NV center are, respectively, $|\psi_{\rm Sky}\rangle = (|0\rangle + |1\rangle)/\sqrt{2}$, $|\psi_{\rm Mag}\rangle = |0\rangle$, and $|\psi_{\rm NV}\rangle = |0\rangle$. When there is no parametric drive [FIG. S12(c)], the quantum state conversion between the two subsystems is impossible. Once the parametric drive is introduced [FIG. S12(d)], the system's coupling strength increases exponentially, allowing quantum state conversion between the two subsystems.

VII. THE SKYRMION-MAGNON-SQ HYBRID SYSTEM

A. The coupling between magnons and SQs

In this section, we will explore the construction of the skyrmion-magnon-SQ hybrid quantum system in detail. The flux-tunable transmon qubit is positioned next to the YIG magnetic sphere, as seen in FIG. S13(a). The energy level of the transmon qubit is depicted in FIG. S13(b). Magnetic stray fields are used to couple the YIG sphere and the superconducting qubit. The interaction between the YIG sphere and the transmon qubit can be described by the

Hamiltonian

$$\hat{H}_{\mathrm{KT}} = \mathcal{J}_{\mathrm{KT}}\left(\hat{c}^{\dagger}\hat{s}_K + h.c.\right) + g_{\mathrm{om}}\hat{c}^{\dagger}\hat{c}\left(\hat{s}_K + \hat{s}_K^{\dagger}\right), \tag{141}$$

where the coupling strength is defined as

$$\begin{aligned}\mathcal{J}_{\mathrm{KT}} &= \frac{\mu_0\mu_{\mathrm{zpf}}}{4\Phi_0^S d_{\mathrm{min}}}\frac{\alpha_J(2E_C E_J^{\mathrm{max}3})^{1/4}}{[S(\phi_b)]^{5/4}},\\ g_{\mathrm{om}} &= \frac{\mu_0\mu_{\mathrm{zpf}}}{16\Phi_0^S d_{\mathrm{min}}}\frac{(1-\alpha_J^2)\sin(2\phi_b)\sqrt{8E_C E_J^{\mathrm{max}}}}{\sqrt{[S(\phi_b)]^3}},\end{aligned} \tag{142}$$

with $\phi_b = \pi\Phi_b/\Phi_0^S$, $E_J^{\mathrm{max}} \equiv E_J^1 - E_J^2$, and $S(\phi_b) = \sqrt{\cos^2\phi_b + \alpha_J^2\sin^2\phi_b}$. α_J, E_J, E_C, Φ_b, and Φ_0^S stand for imbalance between the Josephson energies or superconducting interference device (SQUID) asymmetry, Josephson energies, charging energy, externally applied flux, and the flux quantum, respectively. The first term in Hamiltonian Eq. (141) is the JC interaction, while the second term is analogous to the radiation pressure interaction in an opto-mechanical system. We take typical parameters, which are $R_K = 200$nm for the YIG sphere radius, $d_{\mathrm{min}} = \sqrt{2}R_K$, $\Phi_0^S = h/(2e)$, $E_J^{\mathrm{max}}/h = 50$ GHz, and $E_C/h = 400$ MHz. FIG. S13(c), (d), (e), and (f) show the coupling strengths $\mathcal{J}_{\mathrm{KT}}$ and g_{om} as a function of Φ_b/Φ_0^S. The figures show that parameter Φ_b/Φ_0^S can be used to modulate the coupling strengths $\mathcal{J}_{\mathrm{KT}}$ and g_{om}. In particular, when we choose the parameter $\Phi_b/\Phi_0^S = 0.5$, the coupling strength g_{om} will vanish, meaning that the JC model accurately describes the coupling between the YIG sphere and the superconducting qubit. In the following analysis, we set the value $\Phi_b/\Phi_0^S = 0.5$, and the Hamiltonian Eq. (141) can be simplified to

$$\hat{H}_{\mathrm{KT}} = \mathcal{J}_{\mathrm{KT}}\left(\hat{c}^{\dagger}\hat{s}_K + h.c.\right). \tag{143}$$

Next, we investigate the free Hamiltonian of superconducting qubits, which is denoted by

$$\hat{H}_{\mathrm{Tr}} = \omega_{\mathrm{SQ}}\hat{c}^{\dagger}\hat{c} - \frac{E_C}{2}\hat{c}^{\dagger}\hat{c}\hat{c}^{\dagger}\hat{c}, \tag{144}$$

where E_C denotes the anharmonicity of the qubit energy level and $\omega_{\mathrm{SQ}} = \sqrt{8E_J^{\mathrm{max}}S(\phi_b)E_C} - E_C$ indicates the transmon excitation energy. According to FIG. S13(b), the second nonlinear term (the self-Kerr term) is what causes the energy level of the superconducting qubit to be inhomogeneous. Hence, we can select a qubit made up of the energy levels $|g\rangle$ and $|e\rangle$, whose resonance frequency is $\omega_{\mathrm{Tr}} = \omega_{\mathrm{SQ}}$. FIG. S13(g) and (h) display the resonant frequency ω_{Tr} as a function of Φ_b/Φ_0^S. When α_J is given, ω_{Tr} takes the minimum value at $\Phi_b/\Phi_0^S = 0.5$. In the subsequent analysis, α_J is set to 0.65, at which case the resonant frequency of the qubit $\omega_{\mathrm{Tr}}/2\pi \approx 9.8$ GHz and the coupling strength of the JC interaction $\mathcal{J}_{\mathrm{KT}}/2\pi \approx 2.62$ MHz. The typical qubit relaxation and dephasing times is given by $T_1 = T_2 = 20$ μs, that is, the coupling of superconducting qubits and magnons can reach the strong coupling region.

B. Nonreciprocal excitation conversion between skyrmion qubits and SQs.

The non-reciprocal population conversion between skyrmion qubits and SQs is investigated in this section. Consider a YIG sphere that is coupled to a skyrmion qubit and a SQ and is described by the Hamiltonian

$$\hat{H}_{\mathrm{SKT}} = \omega_K\hat{s}_K^{\dagger}\hat{s}_K + \frac{\omega_q}{2}\hat{\sigma}_z + \frac{\omega_{\mathrm{Tr}}}{2}\hat{\sigma}_z^S + \bar{\lambda}_{\mathrm{KS}}\left(\hat{s}_K\hat{\sigma}_+ + \hat{s}_K^{\dagger}\hat{\sigma}_-\right) + \mathcal{J}_{\mathrm{KT}}\left(\hat{s}_K\hat{\sigma}_+^S + \hat{s}_K^{\dagger}\hat{\sigma}_-^S\right), \tag{145}$$

where the Pauli operators are defined as $\hat{\sigma}_z^S \equiv |e\rangle\langle e| - |g\rangle\langle g|$, $\hat{\sigma}_+^S \equiv |e\rangle\langle g|$, and $\hat{\sigma}_-^S \equiv |g\rangle\langle e|$. Because the radiation pressure coupling term is non-resonant, it is ignored here. The magnon-SQ coupling strength can be made to satisfy $\mathcal{J}_{\mathrm{KT}} = \mathcal{J}_{\mathrm{KT}}^0\cos(\omega_{\mathrm{ac}}t + \phi_e)$ by modulating the external flux ϕ_b, where

$$\mathcal{J}_{\mathrm{KT}}^0 = \frac{\mu_0\mu_{\mathrm{zpf}}}{4\Phi_0^S d_{\mathrm{min}}}\frac{\alpha_J(2E_C E_J^{\mathrm{max}3})^{1/4}}{\hbar}. \tag{146}$$

ω_{ac}, and ϕ_e are the modulation frequency and phase, respectively. When the system is transformed to the rotating frame $U = \exp(i\omega_{ac}t\hat{\sigma}_z^S/2)$, its Hamiltonian is reduced to

$$\hat{H}_{\mathrm{SKT}} = \omega_K\hat{s}_K^{\dagger}\hat{s}_K + \frac{\omega_q}{2}\hat{\sigma}_z + \frac{\Delta_{\mathrm{Tr}}}{2}\hat{\sigma}_z^S + \bar{\lambda}_{\mathrm{KS}}\left(\hat{s}_K\hat{\sigma}_+ + \hat{s}_K^{\dagger}\hat{\sigma}_-\right) + \mathcal{J}_{\mathrm{KT}}^0\left(\hat{s}_K\hat{\sigma}_+^S e^{-i\phi_e} + \hat{s}_K^{\dagger}\hat{\sigma}_-^S e^{i\phi_e}\right), \tag{147}$$

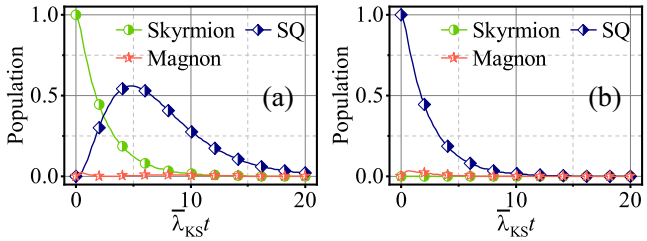

FIG. S14. The population conversion dynamics are presented in (a) and (b), respectively, for excitation of the skyrmion qubit and SQ. The parameters used are $\eta = 1$, $\phi_e = \pi/2$, $\mathcal{G}_{SS} = -\eta\Gamma_{SS}/2$, and $\gamma_K = 10\bar{\lambda}_{KS}$.

where $\Delta_{Tr} \equiv \omega_{Tr} - \omega_{ac}$. Then, going into the interaction picture

$$\hat{H}_{SKT} = \bar{\lambda}_{KS}(\hat{s}_K\hat{\mathfrak{L}}_+ + \hat{s}_K^\dagger\hat{\mathfrak{L}}_-), \tag{148}$$

where $\hat{\mathfrak{L}}_- \equiv \hat{\sigma}_- + \eta\hat{\sigma}_-^S e^{i\phi_e} = \hat{\mathfrak{L}}_+^\dagger$ and $\eta = \mathcal{J}_{KT}^0/(2\bar{\lambda}_{KS})$. The system's master equation is

$$\dot{\hat{\rho}}(t) = -i[\hat{H}_{SKT}, \hat{\rho}] + \gamma_K D[\hat{s}_K]\hat{\rho}. \tag{149}$$

In the bad-cavity limit $\gamma_K \gg \bar{\lambda}_{KS}, \mathcal{J}_{KT}^0$, adiabatically eliminating the magnon modes using the approach described in Sec. V produces

$$\dot{\hat{\rho}} = -i[\hat{H}_{SS}, \hat{\rho}] + \Gamma_{SS} D[\hat{\mathfrak{L}}_-]\hat{\rho}, \tag{150}$$

where $\hat{H}_{SS} = \mathcal{G}_{SS}(\hat{\sigma}_+\hat{\sigma}_-^S + \hat{\sigma}_-\hat{\sigma}_+^S)$ is the coherent coupling between the skyrmion qubit and the SQ, which can be implemented with an auxiliary cavity. The coherent and dissipative coupling strengths are denoted by $\mathcal{G}_{SS}$ and $\Gamma_{SS} = 4\bar{\lambda}_{KS}^2/\gamma_K$, respectively. The system's QLEs can be expressed as

$$\begin{aligned}
\dot{\hat{\sigma}}_- &= -\frac{\Gamma_{SS}}{2}\hat{\sigma}_- + \left(i\mathcal{G}_{SS} + \frac{\Gamma_{SS}}{2}\eta e^{i\phi_e}\right)\hat{\sigma}_-^S\hat{\sigma}_z, \\
\dot{\hat{\sigma}}_-^S &= -\frac{\Gamma_{SS}}{2}\eta^2\hat{\sigma}_-^S + \left(i\mathcal{G}_{SS} + \frac{\Gamma_{SS}}{2}\eta e^{-i\phi_e}\right)\hat{\sigma}_-\hat{\sigma}_z^S.
\end{aligned} \tag{151}$$

It was discovered that by modifying the phase ϕ_e, the competition between coherent and dissipative coupling can be realized, and therefore the asymmetric response between qubits can be accomplished. Specifically, with $\phi_e = \pi/2$ and $\mathcal{G}_{SS} = -\eta\Gamma_{SS}/2$, we get

$$\begin{aligned}
\dot{\hat{\sigma}}_- &= -\Gamma_{SS}/2\hat{\sigma}_-, \\
\dot{\hat{\sigma}}_-^S &= -\Gamma_{SS}/2\eta^2\hat{\sigma}_-^S - i\Gamma_{SS}\eta\hat{\sigma}_-\hat{\sigma}_z^S,
\end{aligned} \tag{152}$$

indicating that the SQ is influenced by the skyrmion qubit and, conversely, the skyrmion qubit is unaffected, implying that complete isolation from SQs to the skyrmion qubits is accomplished. As demonstrated in Fig. S14, the population conversion from SQs to skyrmion qubits is completely isolated.

VIII. ANALYSIS OF EXPERIMENTAL FEASIBILITY BASED ON MICROMAGNETIC SIMULATION

A. Model simplification

The feasibility of the model proposed here will be discussed through micromagnetic simulations. First, a classical picture of the interaction between YIG spheres and skyrmions is described, which will be the basis for performing micromagnetic simulations. Here, we solely take into account the Kittel mode in a YIG sphere, all spins in the micromagnet precessing in phase and with the same amplitude. Moreover, the Kittel mode in YIG spheres can also be described by a macrospin model, meaning that the excitation of magnons can correspond to the precession of macrospins (or magnetic moments). This uniform precession mode leads to a time-dependent field around the magnetic sphere.

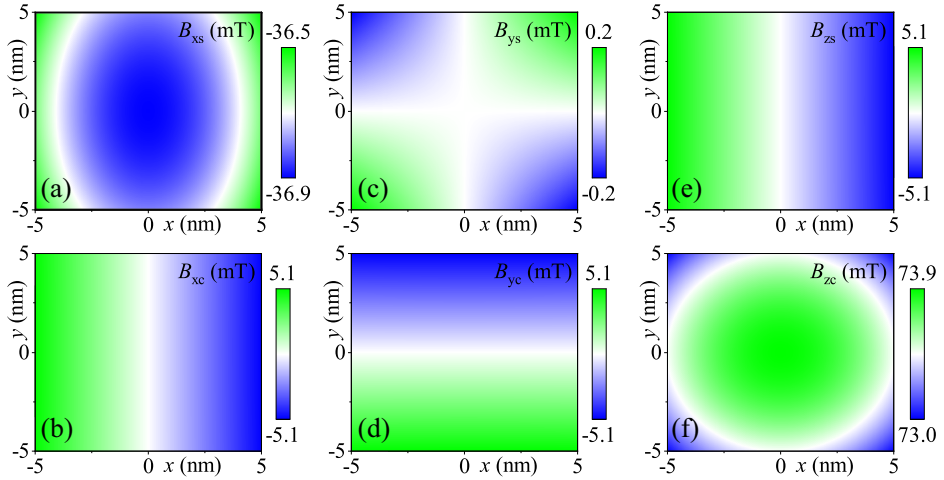

FIG. S15. Spatial envelope of the time-dependent gradient field caused by spin wave excitations.

In this work, $\mathfrak{S}_z$ qubits are considered, and a transition in the quantum state of such a qubit classically corresponds to a change in the z-component of the magnetization, analogous to a change in the charge on the island in a superconducting charge qubit. In other words, in order to verify the coupling of Kittel modes in the YIG sphere and the skyrmion qubit, one can equivalently demonstrate the classical phenomenon that the time-dependent gradient field due to the excitation of the Kittel modes can drive a variation of the z-component magnetization of the skyrmion.

Next, the time-dependent gradient field due to the excitation of the Kittel mode is derived. In the manuscript, we consider the magnetic sphere being magnetized along the y direction. The classical mode function describing the Kittel mode is given as $\boldsymbol{m}(\boldsymbol{r},t) = m\,(\boldsymbol{e}_z + i\boldsymbol{e}_x)\,e^{-i\omega t} + c.c.$, where m represents the amplitude of precession, which satisfies the condition $m \ll M_s$. The time-dependent gradient field caused by the precession of the magnetic moment can be calculated using the magnetic dipole model

$$\boldsymbol{B}(\boldsymbol{r},t) = \frac{\mu_0}{4\pi}\left[\frac{\boldsymbol{r}(\boldsymbol{\mu}\cdot\boldsymbol{r})}{r^5} - \frac{\boldsymbol{\mu}}{r^3}\right] \tag{153}$$

with $\boldsymbol{\mu}(\boldsymbol{r},t) = \boldsymbol{m}(\boldsymbol{r},t)V_K$ and $r = \sqrt{x^2+y^2+h_K^2}$. After algebraic calculation, each component of the time-dependent gradient field can be written as

$$B_x(\boldsymbol{r},t) = B_{\rm xs}\sin\omega t + B_{\rm xc}\cos\omega t, \tag{154a}$$

$$B_y(\boldsymbol{r},t) = B_{\rm ys}\sin\omega t + B_{\rm yc}\cos\omega t, \tag{154b}$$

$$B_z(\boldsymbol{r},t) = B_{\rm zs}\sin\omega t + B_{\rm zc}\cos\omega t, \tag{154c}$$

where

$$B_{\rm xs} = \frac{2m\mu_0 V_K}{4\pi}\left(\frac{3x^2}{r^5} - \frac{1}{r^3}\right),\ B_{\rm xc} = -\frac{2m\mu_0 V_K}{4\pi}\frac{3h_K x}{r^5}, \tag{155a}$$

$$B_{\rm ys} = \frac{2m\mu_0 V_K}{4\pi}\frac{3xy}{r^5},\ B_{\rm yc} = -\frac{2m\mu_0 V_K}{4\pi}\frac{3h_K y}{r^5}, \tag{155b}$$

$$B_{\rm zs} = -\frac{2m\mu_0 V_K}{4\pi}\frac{3xh_K}{r^5},\ B_{\rm zc} = \frac{2m\mu_0 V_K}{4\pi}\left(\frac{3h_K^2}{r^5} - \frac{1}{r^3}\right). \tag{155c}$$

Next we simplify the time-dependent gradient field (154). For a magnetic sphere with a radius $R_K = 100$ nm and a precession amplitude $m = 0.1M_s$ for the Kittel mode, the spatial envelope of the time-dependent gradient field experienced by the skyrmion is illustrated in Fig. S15. It can be easily noticed that $\{B_{\rm xs}, B_{\rm zc}\} \gg \{B_{\rm xc}, B_{\rm ys}, B_{\rm yc}, B_{\rm zs}\}$,

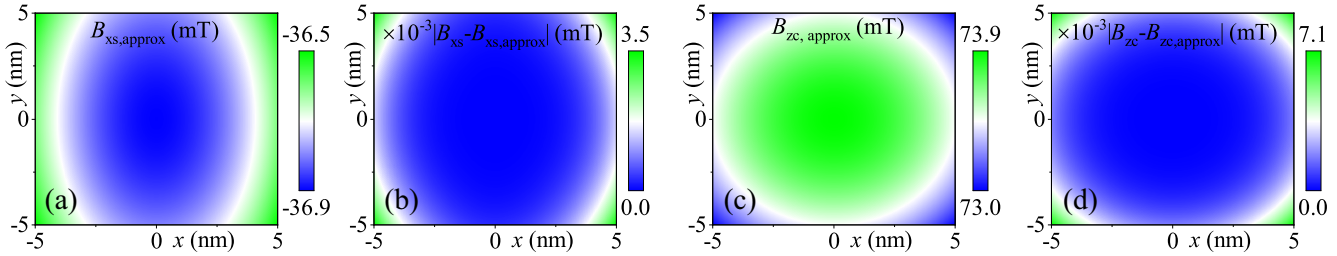

FIG. S16. The approximate solutions $B_{\rm xs,approx}$ and $B_{\rm zc,approx}$ and their errors are respectively depicted in (a) and (b), and (c) and (d).

meaning $B_{\rm xs}$ and $B_{\rm zc}$ provide the main contributions, and the contributions of other terms can be neglected. Therefore, Eq. (154) can be simplified to

$$B_x(\boldsymbol{r},t) = B_{\rm xs}\sin\omega t,\ \ B_y(\boldsymbol{r},t) = 0,\ \ B_z(\boldsymbol{r},t) = B_{\rm zc}\cos\omega t. \tag{156}$$

The spatial envelopes of $B_{\rm xs}$ and $B_{\rm zc}$, as observed in Figs. S15(a) and (f), are paraboloidal and can be simplified using series expansion. Retaining terms up to the second order, $B_{\rm xs}$ and $B_{\rm zc}$ simplify to

$$B_{\rm xs,approx} \approx \frac{2m\mu_0 V_K}{4\pi}\left(-\frac{1}{h_K^3} + \frac{9}{2h_K^5}x^2 + \frac{3}{2h_K^5}y^2\right), \tag{157a}$$

$$B_{\rm zc,approx} \approx \frac{2m\mu_0 V_K}{4\pi}\left(\frac{2}{h_K^3} - \frac{6}{h_K^5}x^2 - \frac{6}{h_K^5}y^2\right). \tag{157b}$$

Figure S16 displays the field envelopes described by the approximate expressions $B_{\rm xs,approx}$ and $B_{\rm zc,approx}$, along with their deviation from the exact solution, demonstrating that the approximate expressions derived from the series expansion effectively characterize the spatial envelope of the field. The zeroth-order term in the approximate expression represents a uniform field. The in-plane time-dependent uniform field does not affect the dynamics of skyrmion qubits and can be ignored; however, the out-of-plane time-dependent uniform field does affect the dynamics of skyrmion qubits and cannot be ignored. By redefining constants and using the width of the skyrmion $w_{\rm Sky} = 8.4$ nm (Sec. VIII B) as the length scale, the final simplified model of the magnetic field induced by magnon excitation $\boldsymbol{B} = (B_x, 0, B_z)$ is obtained as

$$B_x = B_x^0(3x^2+y^2)\sin\omega t,\ \ B_z = B_z^u\cos\omega t - B_z^0(x^2+y^2)\cos\omega t, \tag{158}$$

where

$$B_x^0 = \frac{3m\mu_0 V_K}{4\pi h^5},\ \ B_z^u = \frac{m\mu_0 V_K}{\pi h^3},\ \ B_z^0 = \frac{3m\mu_0 V_K}{\pi h^5},\ \ h = \frac{h_K}{w_{\rm Sky}}. \tag{159}$$

B. Micromagnetic simulation

To simulate the dynamics of the skyrmion qubit induced by a time-dependent gradient magnetic field resulting from the excitation of the magnon mode in the YIG sphere, we consider a two-dimensional ferromagnetic film with exchange frustration based on the J_1-J_2-J_3 classical Heisenberg model on a simple square lattice [17–20],

$$\begin{aligned}\mathcal{H} = &-J_1\sum_{<i,j>}\boldsymbol{m}_i\cdot\boldsymbol{m}_j - J_2\sum_{\ll i,j\gg}\boldsymbol{m}_i\cdot\boldsymbol{m}_j - J_3\sum_{\lll i,j\ggg}\boldsymbol{m}_i\cdot\boldsymbol{m}_j\\ &-K\sum_i(m_i^z)^2 - M_{\rm S}\sum_i\boldsymbol{B}\cdot\boldsymbol{m}_i - \frac{1}{2}M_{\rm S}\sum_i\boldsymbol{B}_{\rm D}\cdot\boldsymbol{m}_i,\end{aligned} \tag{160}$$

where $\boldsymbol{m}_i = \boldsymbol{M}_i/M_{\rm S}$ represents the normalized spin at the site i with $M_{\rm S}$ being the saturation magnetization, i.e., $|\boldsymbol{m}_i| = 1$. J_1, J_2, and J_3 denote the ferromagnetic nearest-neighbor (NN), antiferromagnetic next-NN (NNN), and antiferromagnetic next-NNN (NNNN) intralayer exchange interaction constants, respectively. $\langle i,j\rangle$, $\langle\langle i,j\rangle\rangle$, and

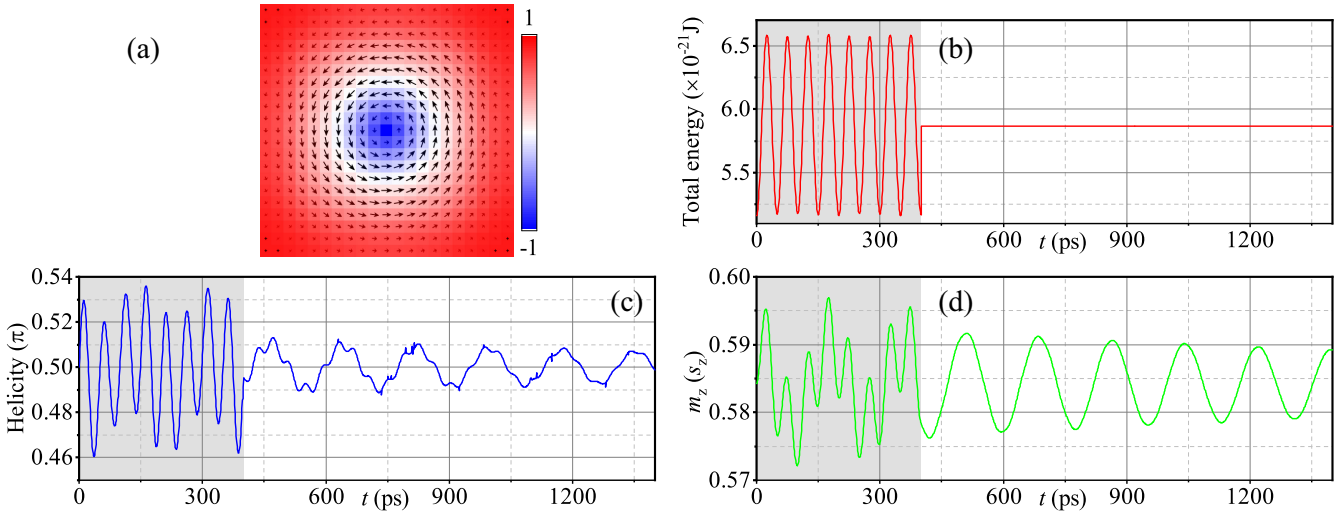

FIG. S17. (a) The initial state of the skyrmion, with a helicity of $\pi/2$. (b), (c), and (d) respectively depict the temporal evolution of the skyrmions total energy, the helicity, and the z-component magnetization. The shaded regions denote the presence of a time-dependent gradient field, which persists for 400 ps.

$\langle\langle\langle i,j\rangle\rangle\rangle$ run over all the NN, NNN, and NNNN sites in the ferromagnetic layer, respectively. K is the perpendicular magnetic anisotropy (PMA) constant. $\boldsymbol{B}$ is the applied external magnetic field. $\boldsymbol{B}_{\rm D}$ is the demagnetizing field resulting from the dipole-dipole interaction. Note that the dipole-dipole interaction favors the Bloch-type skyrmions with the helicity values of $\eta = \pi/2$ and $\eta = 3\pi/2$. The spin dynamics driven by the magnetic field is described by the Landau-Lifshitz-Gilbert equation [21]

$$\frac{d\boldsymbol{m}}{dt} = -\gamma_0 \boldsymbol{m} \times \boldsymbol{h}_{\rm eff} + \alpha \left(\boldsymbol{m} \times \frac{d\boldsymbol{m}}{dt} \right), \tag{161}$$

where $\boldsymbol{h}_{\rm eff} = -\frac{1}{\mu_0 M_{\rm S}} \cdot \frac{\delta \mathcal{H}}{\delta \boldsymbol{m}}$ is the effective field, μ_0 is the vacuum permeability constant, t is the time, α is the Gilbert damping parameter, and γ_0 is the absolute gyromagnetic ratio. The simulation parameters are [19, 20]: $J_1 = 3$ meV, $J_2 = -0.8$ (in units of $J_1 = 1$), $J_3 = -0.6$ (in units of $J_1 = 1$), $K = 0.005$ (in units of $J_1/a^3 = 1$), $\alpha = 0.01$, $\gamma_0 = 2.211 \times 10^5$ m A^{-1} s^{-1}, and $M_{\rm S} = 580$ kA m^{-1}. The lattice constant is $a = 0.4$ nm, and thus the cell size is a^3. The simulated model is a square film with 21×21 spins, that is, the length and width are equal to 8.4 nm. We also assume that the edge spins have enhanced PMA of $K = 0.05$ in order to confine the frustrated skyrmion. The simulation is carried out by using the Object Oriented MicroMagnetic Framework (OOMMF) [22] upgraded with our extension modules to simulate the model.

In the simulation, we first apply a time-dependent gradient magnetic field to drive the dynamics of a relaxed frustrated skyrmion at the square film center. The initial helicity state of the skyrmion is $\eta = \pi/2$. For the sake of simplicity, we assume that the profile of the time-dependent gradient magnetic field is $\boldsymbol{B} = (B_x, 0, B_z)$ with $B_x = B_x^0(3x^2 + y^2)\sin(2\pi f t)$ and $B_z = B_z^u \cos(2\pi f t) - B_z^0(x^2 + y^2)\cos(2\pi f t)$. We assume a frequency of $f = 20$ GHz and field strength parameters of $B_x^0 = 0.32$ mT, $B_z^0 = 1.29$ mT, and $B_z^u = 73.89$ mT. The time-dependent gradient magnetic field is applied for 400 ps during $t = 0 - 400$ ps, followed by a 1000-ps-long relaxation without the magnetic field. Namely, the total simulation time is 1400 ps.

C. Results and discussion

The results of the micromagnetic simulation are presented in Fig. S17. The initial state of the skyrmion, with a helicity $\pi/2$, is depicted in Fig. S17(a). As discussed in Sec. VIII A, the classical correspondence of the interaction between magnons and skyrmion qubits is as follows: the excitation of magnons leads to the generation of a time-dependent gradient field, which influences the dynamics of skyrmions. Here, we focus on $\mathfrak{S}_z$ qubits, where the transitions of their quantum states correspond to changes in the z component of the skyrmion's magnetization, while the helicity oscillates around its equilibrium position. Simultaneously, transitions in the quantum states correspond to changes in the system's energy, the classical analog of which is the change in the total energy of the skyrmion. As described in Sec. VIII B, the interaction between the magnon and the skyrmion qubit is simulated by applying

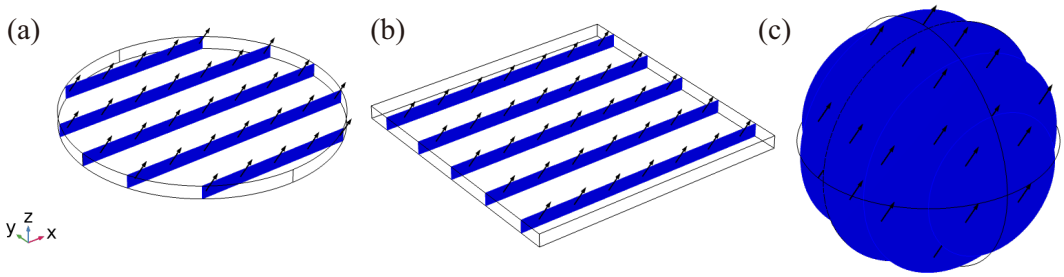

FIG. S18. Spin wave eigenmodes are identified using the finite element simulation software COMSOL. Panels (a), (b), and (c) illustrate the uniform precession modes, known as Kittel modes, in a circular dot (radius $R_c = 100$ nm and thickness $c = 10$ nm), a square dot (width $w = 200$ nm and thickness $c = 10$ nm), and a YIG sphere (radius $R_K = 100$ nm), respectively. In COMSOL, the YIG material parameters are defined with values Gilbert damping $\alpha = 5 \times 10^{-4}$, saturation magnetization $M_s = 587$ kA/m, exchange coefficient $A_{\rm ex} = 0.328 \times 10^{-10}$ A/m, and magnetic crystal anisotropy $K_{\rm an} = 0.385 \times 10^5$ A/m.

the time-dependent gradient field (158). After 400 ps, the time-dependent gradient field is removed to simulate the relaxation process of the skyrmion qubit. As shown in Figs. S17(b, c, d), when the time-dependent gradient field exists, the total energy of the skyrmion, the helicity, and the z component of the magnetization all oscillate over time; when the time-dependent gradient field is removed (i.e., the skyrmion qubits are not coupled to the magnons), it can be seen that the total energy of the skyrmion, the helicity, and the z component of the magnetization all gradually relax to the steady state, and after a sufficiently long time, they will relax back to the initial steady state.

In summary, using micromagnetism simulations, we demonstrate the feasibility of the scheme proposed here. All the simulations here are based on the YIG magnetic sphere, but these results are equally valid for the magnetic multilayer structure discussed later.

IX. MAGNETIC MULTILAYER CONFIGURATIONS

A. Micromagnetic simulations of spin waves

In the preceding discussions, Kittel modes in spherical YIG materials are highlighted. Additionally, spin wave behaviors in non-spherical magnetic geometries have received extensive attention. Here we focus on the uniform precession mode in square and circular dots, which corresponds to the case $\boldsymbol{k} = 0$ [2]. The orientation of magnetization presents two scenarios: perpendicular to the dot plane, and within the dot plane. For the former, the resonance frequency, denoted as $\omega = \omega_0 = |\gamma|\mu_0(H - M_s)$, while for the latter, designated as $\omega = \sqrt{\omega_0(\omega_0 + \omega_M)}$ [2]. These are defined where M_s represents the saturation magnetization, H is the applied field, and $\omega_M = |\gamma|\mu_0 M_s$. To validate these uniform precession modes, we conducted simulations using micromagnetic techniques. In these simulations, YIG material was selected for its small magnetic damping $\alpha = 10^{-4} \sim 10^{-5}$.

Initially, eigenmodes in the circular dot, square dot, and YIG sphere were investigated using the finite element simulation software COMSOL, as depicted in Fig. S18. This analysis confirmed the presence of uniform precession modes, namely Kittel modes, in each geometry. Subsequent simulations, employing the micromagnetic software mumax3 [23], focused on spin wave excitation via a magnetic field pulse. These simulations exclusively addressed classical spin waves. Figures S19(a) and (b) reveal that the Kittel mode in both circular and square dots follows an elliptical, rather than circular, precession trajectory. This elliptical precession is attributed to the thinness in the z-direction of these dots, resulting in surface spin behavior akin to pinning, which impedes circular precession. In contrast, the heightened symmetry of the YIG sphere facilitates circular precession trajectories for its Kittel modes, as shown in Fig. S19(c).

B. Magnon-skyrmion qubit coupling

This section focuses on the two models depicted in Fig. S20, with an emphasis on calculating their coupling strengths. Here, a magnetic dot is separated from the skyrmion by a spacer, its thickness indicated as $l = 5$ nm. The interaction between the magnons and skyrmions occurs through a magnetic field. The magnetic dots are magnetized in the y direction. Given that the calculation methodology for coupling strength is identical for both square and circular dots,

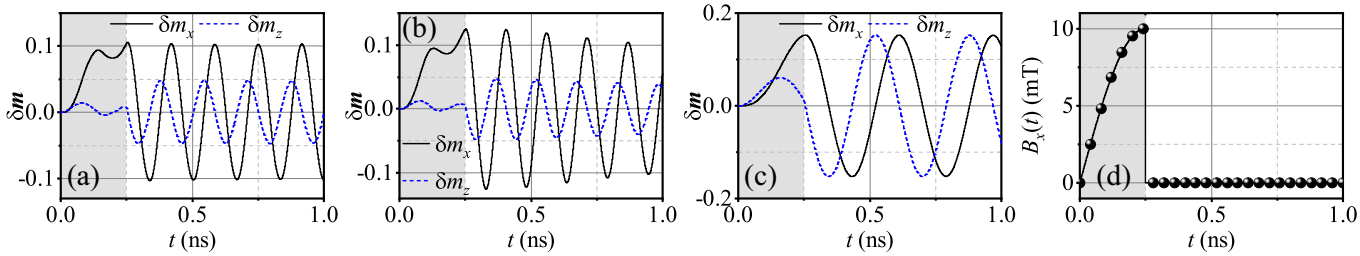

FIG. S19. Figures (a), (b), and (c) respectively represent the excited Kittel modes in a circular dot (radius $R_c = 100$ nm and thickness $c = 20$ nm), a square dot (width $w = 100$ nm and thickness $c = 10$ nm), and a YIG sphere (radius $R_K = 100$ nm). The shaded regions in the figure correspond to areas with an applied driving magnetic field. Figure (d) illustrates the magnetic field applied during the complete evolution. For $t \leq 0.25$ ns, the magnetic field is set to $\boldsymbol{B} = (B_0 \sin \omega t, B_y, 0)$; for $t > 0.25$ ns, it is defined as $\boldsymbol{B} = (0, B_y, 0)$, where $B_0 = 10$ mT, $\omega/2\pi = 1$ GHz, and $B_y = 0.1$ T.

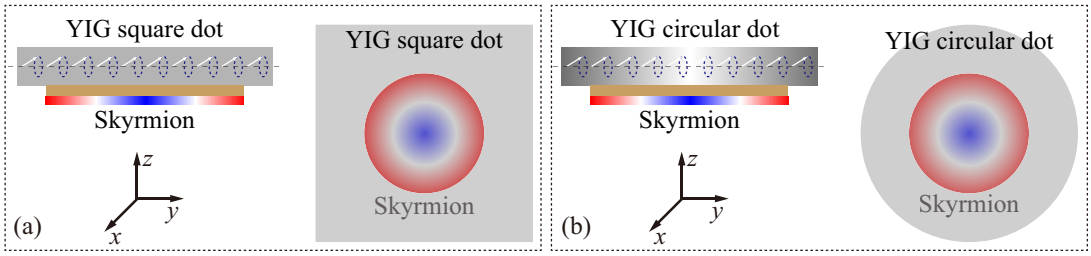

FIG. S20. Figures (a) and (b) respectively present models of square and circular dots coupled with skyrmion qubits, with the YIG dot and the skyrmion separated by a spacer.

the analysis in this instance will use square dots as a representative example to examine the coupling strength between the magnon and the skyrmion qubit.

This analysis considers a square dot characterized by dimensions (w, w, c), where w represents the width and c denotes the thickness. To calculate the magnetic field impacting the skyrmion qubit, generated by this square dot, a discretization approach is applied. Within this framework, the magnetic field from each volumetric microelement of the dot is estimated using a magnetic dipole model

$$\boldsymbol{B}_{\mathrm{SD}} = \frac{\mu_0 dV_{\mathrm{SD}}}{4\pi} \left[\frac{3\boldsymbol{r}_{\mathrm{SD}} \cdot (\boldsymbol{M}_{\mathrm{SD}} \cdot \boldsymbol{r}_{\mathrm{SD}})}{r_{\mathrm{SD}}^5} - \frac{\boldsymbol{M}_{\mathrm{SD}}}{r_{\mathrm{SD}}^3} \right] \tag{162}$$

with $\boldsymbol{r}_{\mathrm{SD}} = (x - x_s, y - y_s, -z_s)$. The distance from any point of the square dot to the skyrmion is $r_{\mathrm{SD}} = \sqrt{(x - x_s)^2 + (y - y_s)^2 + z_s^2}$, where the coordinates of any point of the square dot are (x_s, y_s, z_s). Following the quantization process of the spin wave in Sec. I, we can introduce the quantum magnetization operator $\hat{\boldsymbol{M}}_{\mathrm{SD}} = M_{\mathrm{SD}}(\widetilde{\boldsymbol{m}}_{\mathrm{SD}} \hat{s}_{\mathrm{SD}} + \widetilde{\boldsymbol{m}}_{\mathrm{SD}}^* \hat{s}_{\mathrm{SD}}^\dagger)$ with $\widetilde{\boldsymbol{m}}_{\mathrm{SD}} = \eta_e \hat{\boldsymbol{e}}_z + i\hat{\boldsymbol{e}}_x$, where for a square dot, the zero-point magnetization can be written as $M_{\mathrm{SD}} = \sqrt{\hbar\gamma_e M_s/(2V_{\mathrm{SD}})}$ with $V_{\mathrm{SD}} = w^2 c$. The parameter η_e indicates that the trajectory is an ellipse. Depending on the results in Fig. S19(b), η_e can be approximated as 0.5. Then the quantized magnetic field in each

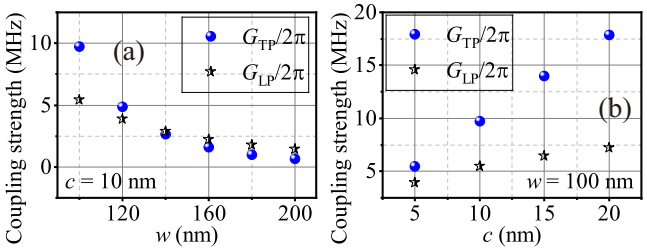

FIG. S21. (a) illustrates the variation of coupling strength with the width w of the square dot. (b) delineates the coupling strength's dependence on the thickness c of the square dot.

direction can be expressed as

$$\hat{B}_x = \frac{\mu_0 d V_{\rm SD} M_{\rm SD}}{4\pi}\left\{\frac{3\left[i\left(\hat{s}_{\rm SD}-\hat{s}^\dagger_{\rm SD}\right)(x-x_s)-z_s\eta_e\left(\hat{s}_{\rm SD}+\hat{s}^\dagger_{\rm SD}\right)\right]}{r^5_{\rm SD}}(x-x_s)-\frac{i\left(\hat{s}_{\rm SD}-\hat{s}^\dagger_{\rm SD}\right)}{r^3_{\rm SD}}\right\}, \tag{163a}$$

$$\hat{B}_y = \frac{\mu_0 d V_{\rm SD} M_{\rm SD}}{4\pi}\left\{\frac{3\left[i\left(\hat{s}_{\rm SD}-\hat{s}^\dagger_{\rm SD}\right)(x-x_s)-z_s\eta_e\left(\hat{s}_{\rm SD}+\hat{s}^\dagger_{\rm SD}\right)\right]}{r^5_{\rm SD}}(y-y_s)\right\}, \tag{163b}$$

$$\hat{B}_z = \frac{\mu_0 d V_{\rm SD} M_{\rm SD}}{4\pi}\left\{\frac{3\left[i\left(\hat{s}_{\rm SD}-\hat{s}^\dagger_{\rm SD}\right)(x-x_s)-z_s\eta_e\left(\hat{s}_{\rm SD}+\hat{s}^\dagger_{\rm SD}\right)\right]}{r^5_{\rm SD}}(-z_s)-\frac{\left(\hat{s}_{\rm SD}-\hat{s}^\dagger_{\rm SD}\right)}{r^3_{\rm SD}}\right\}. \tag{163c}$$

According to Sec. III B, the interaction Hamiltonian can be given by

$$\hat{H}_{\rm SDK} = -\frac{g\mu_B\bar{S}}{a^2}\int_{V_{\rm SD}}\int d\boldsymbol{r}\boldsymbol{B}_{\rm SD}\cdot\boldsymbol{s}. \tag{164}$$

After a similar algebraic process as in Sec. III B, the interaction Hamiltonian can be reduced to

$$\hat{H}_{\rm SDK} = iG_{\rm TM}\left(\hat{s}_{\rm SD}\hat{\sigma}_+ - \hat{s}^\dagger_{\rm SD}\hat{\sigma}_-\right)+G_{\rm TP}\eta_e\left(\hat{s}_{\rm SD}\hat{\sigma}_+ + \hat{s}^\dagger_{\rm SD}\hat{\sigma}_-\right)+iG_{\rm LM}\left(\hat{s}_{\rm SD}-\hat{s}^\dagger_{\rm SD}\right)\hat{\sigma}_z+G_{\rm LP}\eta_e\left(\hat{s}_{\rm SD}+\hat{s}^\dagger_{\rm SD}\right)\hat{\sigma}_z, \tag{165}$$

where the counter-rotating terms have been ignored. The coupling strengths are denoted as $G_{\rm TM} = 1/2[(g^1_x+g^1_y)-(g^4_x+g^4_y)]$, $G_{\rm TP} = 1/2[(g^2_x+g^2_y)+(g^3_x+g^3_y)]$, $G_{\rm LM} = 1/2g^1_z$, and $G_{\rm LP} = 1/2g^2_z$. The detailed expressions of $g^{1,2,3,4}_{x,y}$ and $g^{1,2}_z$ in the coupling strength are

$$g^1_x = -\frac{\mu_0 M_{\rm SD}}{4\pi}g\mu_B\bar{S}\int dx_s\int dy_s\int dz_s\int d\rho\int d\phi\rho\left[\left(\frac{3(x-x_s)^2}{r^5_{\rm SD}}-\frac{1}{r^3_{\rm SD}}\right)\sin\Theta_0\cos\phi\right], \tag{166a}$$

$$g^2_x = \frac{\mu_0 M_{\rm SD}}{4\pi}g\mu_B\bar{S}\int dx_s\int dy_s\int dz_s\int d\rho\int d\phi\rho\left[\left(\frac{3(x-x_s)^2}{r^5_{\rm SD}}-\frac{1}{r^3_{\rm SD}}\right)\sin\Theta_0\sin\phi\right], \tag{166b}$$

$$g^3_x = \frac{\mu_0 M_{\rm SD}}{4\pi}g\mu_B\bar{S}\int dx_s\int dy_s\int dz_s\int d\rho\int d\phi\rho\left[\frac{3z_s}{r^5_{\rm SD}}(x-x_s)\sin\Theta_0\cos\phi\right], \tag{166c}$$

$$g^4_x = -\frac{\mu_0 M_{\rm SD}}{4\pi}g\mu_B\bar{S}\int dx_s\int dy_s\int dz_s\int d\rho\int d\phi\rho\left[\frac{3z_s}{r^5_{\rm SD}}(x-x_s)\sin\Theta_0\sin\phi\right], \tag{166d}$$

$$g^1_y = -\frac{\mu_0 M_{\rm SD}}{4\pi}g\mu_B\bar{S}\int dx_s\int dy_s\int dz_s\int d\rho\int d\phi\rho\left[\frac{3(x-x_s)}{r^5_{\rm SD}}(y-y_s)\sin\Theta_0\sin\phi\right], \tag{166e}$$

$$g^2_y = -\frac{\mu_0 M_{\rm SD}}{4\pi}g\mu_B\bar{S}\int dx_s\int dy_s\int dz_s\int d\rho\int d\phi\rho\left[\frac{3(x-x_s)}{r^5_{\rm SD}}(y-y_s)\sin\Theta_0\cos\phi\right], \tag{166f}$$

$$g^3_y = \frac{\mu_0 M_{\rm SD}}{4\pi}g\mu_B\bar{S}\int dx_s\int dy_s\int dz_s\int d\rho\int d\phi\rho\left[\frac{3z_s}{r^5_{\rm SD}}(y-y_s)\sin\Theta_0\sin\phi\right], \tag{166g}$$

$$g^4_y = \frac{\mu_0 M_{\rm SD}}{4\pi}g\mu_B\bar{S}\int dx_s\int dy_s\int dz_s\int d\rho\int d\phi\rho\left[\frac{3z_s}{r^5_{\rm SD}}(y-y_s)\sin\Theta_0\cos\phi\right], \tag{166h}$$

$$g_z^1 = -\frac{\mu_0 M_{\rm SD}}{4\pi}\frac{g\mu_B \bar{S}}{\Lambda}\int dx_s \int dy_s \int dz_s \int d\rho \int d\phi\rho \left[\frac{3(x-x_s)}{r_{\rm SD}^5} z_s(1-\cos\Theta_0)\right], \tag{166i}$$

$$g_z^2 = \frac{\mu_0 M_{\rm SD}}{4\pi}\frac{g\mu_B \bar{S}}{\Lambda}\int dx_s \int dy_s \int dz_s \int d\rho \int d\phi\rho \left[\frac{3z_s^2}{r_{\rm SD}^5} - \frac{1}{r_{\rm SD}^3}\right](1-\cos\Theta_0). \tag{166j}$$

We have dimensionlessized the integral in the expression using the lattice constant a. Taking the parameters $w = 100$ nm ~ 200 nm and $c = 5$ nm ~ 20 nm, the coupling strength can be obtained via numerical calculations as shown in Fig. S21. Numerical calculations shows $G_{\rm TM} \approx 0$ and $G_{\rm LM} \approx 0$. Figure S21(a) illustrates that the coupling strength decreases as the width w of the square dots increases, while Figs. S21(b) shows that the coupling strength increases as the thickness c of the square dots increases. Figure S21 also demonstrates that the coupling of square dots and skyrmion qubits can reach the strong-coupling region ($G_{\rm TP}/2\pi, G_{\rm LP}/2\pi > \max\{\gamma_{\rm Sky}, \gamma_K\}$). In other words, strong coupling of magnons and skyrmion qubits is experimentally feasible in the magnetic multilayer structure (Fig. S20).

[1] A. Aharoni, *Introduction to the Theory of Ferromagnetism* (Clarendon Press, Oxford, 2000).
[2] D. D. Stancil and A. Prabhakar, *Spin waves: Theory and applications* (Springer US, New York, 2009).
[3] J. D. Jackson, *Classical electrodynamics* (Wiley, New York, 1975).
[4] P. C. Fletcher and R. O. Bell, Ferrimagnetic resonance modes in spheres, J. Appl. Phys. **30**, 687 (1959).
[5] P. Röschmann and H. Dötsch, Properties of magnetostatic modes in ferrimagnetic spheroids, Phys. Status Solidi B **82**, 11 (1977).
[6] L. R. Walker, Magnetostatic modes in ferromagnetic resonance, Phys. Rev. **105**, 390 (1957).
[7] D. Mills, Quantum theory of spin waves in finite samples, J. Magn. Magn. Mater. **306**, 16 (2006).
[8] H.-B. Braun and D. Loss, Berry's phase and quantum dynamics of ferromagnetic solitons, Phys. Rev. B **53**, 3237 (1996).
[9] S. Chaki and A. Bhattacherjee, Role of dissipation in the stability of a parametrically driven quantum harmonic oscillator, J. Korean Phys. Soc. **79**, 600 (2021).
[10] D. Nwaigwe, On the convergence of WKB approximations of the damped Mathieu equation, J. Math. Phys. **62**, 062702 (2021).
[11] T. Holstein and H. Primakoff, Field dependence of the intrinsic domain magnetization of a ferromagnet, Phys. Rev. **58**, 1098 (1940).
[12] P.-B. Li, S.-Y. Gao, and F.-L. Li, Quantum-information transfer with nitrogen-vacancy centers coupled to a whispering-gallery microresonator, Phys. Rev. A **83**, 054306 (2011).
[13] Y.-D. Wang and A. A. Clerk, Using interference for high fidelity quantum state transfer in optomechanics, Phys. Rev. Lett. **108**, 153603 (2012).
[14] S. D. Bennett, N. Y. Yao, J. Otterbach, P. Zoller, P. Rabl, and M. D. Lukin, Phonon-induced spin-spin interactions in diamond nanostructures: Application to spin squeezing, Phys. Rev. Lett. **110**, 156402 (2013).
[15] B. Li, P.-B. Li, Y. Zhou, S.-L. Ma, and F.-L. Li, Quantum microwave-optical interface with nitrogen-vacancy centers in diamond, Phys. Rev. A **96**, 032342 (2017).
[16] B. Li, P.-B. Li, Y. Zhou, J. Liu, H.-R. Li, and F.-L. Li, Interfacing a topological qubit with a spin qubit in a hybrid quantum system, Phys. Rev. Appl. **11**, 044026 (2019).
[17] C. D. Batista, S.-Z. Lin, S. Hayami, and Y. Kamiya, Frustration and chiral orderings in correlated electron systems, Rep. Prog. Phys. **79**, 084504 (2016).
[18] H. T. Diep, Phase transition in frustrated magnetic thin filmphysics at phase boundaries, Entropy **21**, 175 (2019).
[19] X. Zhang, J. Xia, L. Shen, M. Ezawa, O. A. Tretiakov, G. Zhao, X. Liu, and Y. Zhou, Static and dynamic properties of bimerons in a frustrated ferromagnetic monolayer, Phys. Rev. B **101**, 144435 (2020).
[20] X. Zhang, J. Xia, O. A. Tretiakov, H. T. Diep, G. Zhao, J. Yang, Y. Zhou, M. Ezawa, and X. Liu, Dynamic transformation between a skyrmion string and a bimeron string in a layered frustrated system, Phys. Rev. B **104**, L220406 (2021).
[21] T. Gilbert, A phenomenological theory of damping in ferromagnetic materials, IEEE Trans. Magn. **40**, 3443 (2004).
[22] M. J. Donahue and D. G. Porter, OOMMF User's Guide, Version 1.0, Interagency Report NO. NISTIR 6376 (National Institute of Standards and Technology, Gaithersburg, MD, 1999).
[23] A. Vansteenkiste, J. Leliaert, M. Dvornik, M. Helsen, F. Garcia-Sanchez, and B. Van Waeyenberge, The design and verification of Mumax3, AIP Adv. **4**, 107133 (2014).